THE ASTROPHYSICAL JOURNAL, 397:304–328, 1992 September 20

ANALYSIS OF THE PHOTOSPHERIC EPOCH SPECTRA OF TYPE Ia SUPERNOVAE SN 1990N AND SN 1991T[1]

DAVID J. JEFFERY, BRUNO LEIBUNDGUT, AND ROBERT P. KIRSHNER
Harvard-Smithsonian Center for Astrophysics, MS-19, 60 Garden Street, Cambridge, MA 02138
STEFANO BENETTI[2] AND DAVID BRANCH
Department of Physics and Astronomy, University of Oklahoma, Norman, OK 73019
AND
GEORGE SONNEBORN
Laboratory for Astronomy and Solar Physics, NASA/Goddard Space Flight Center, Code 681, Greenbelt, MD 20771
Received 1992 January 23; accepted 1992 March 27

ABSTRACT

An analysis of the photospheric epoch optical and UV spectra (obtained with the *IUE* satellite) of Type Ia supernovae SN 1990N and SN 1991T is presented. To perform the analysis, synthetic spectra calculated using an LTE radiative transfer procedure and white dwarf explosion models of Type Ia supernovae were fitted to the observations. For both supernovae, the observed spectra are consistent with a white dwarf explosion model that possesses a core of newly synthesized iron peak elements, a core boundary moving at $\sim$9000 km s^{-1}, and an envelope with a composition of intermediate-mass elements. In the well known white dwarf explosion model W7, the inner envelope (i.e., matter with velocities in the range $\sim$9000–15,000 km s^{-1}) consists of newly synthesized elements produced as the burning front of the explosion died out. For SN 1990N the observed spectra are consistent with a composition of the inner envelope that is like that of model W7. For SN 1991T the observed spectra suggest that the inner envelope of this supernova has silicon underabundant by a factor of order 3 and calcium underabundant by a factor of order 10 relative to model W7. The near-UV spectra (2500–3500 Å) for both supernovae are best fitted by assuming that there are iron peak elements in the ejecta moving at velocities greater than 15,000 km s^{-1} (i.e., in the outer envelope) and that these iron peak elements are dominated by newly synthesized Ni-Co. This result is inconsistent with the model W7 prediction of an outer envelope consisting of unburned matter dominated by carbon and oxygen. The absolute abundance of intermediate-mass elements in the outer ejecta is quite uncertain for both supernovae, but spectrum fitting shows that abundances higher than solar are probable and suggests that silicon, sulfur, and calcium are underabundant in SN 1991T relative to SN 1990N by factors of order 3, 3, and 10, respectively. In the case of SN 1990N, there are ejecta moving at a velocity of $\sim$40,000 km s^{-1} and newly synthesized material moving perhaps as fast as 25,000 km s^{-1}. SN 1991T has matter moving at least as fast as $\sim$20,000 km s^{-1}. Model W7 has no ejecta moving faster than 22,027 km s^{-1}. Some variation on model W7 or the delayed/late detonation models for Type Ia supernovae may be able to explain the high velocities required for SN 1990N and the newly synthesized elements that are probably present in the outer ejecta of both supernovae. The synthetic spectra calculated for the analysis and the expanding photosphere method are used for absolute *B* maximum and distance determinations for SN 1990N and SN 1991T.

Subject headings: stars: abundances — supernovae: individual (SN 1990N, SN 1991T) — techniques: spectroscopic

1. INTRODUCTION

In this paper, a local thermodynamic equilibrium (LTE) analysis is done of the photospheric epoch optical and *IUE* UV spectra of the recent and well-observed Type Ia supernovae SN 1990N (Liebundgut et al. 1991a) and SN 1991T (Filippenko et al. 1992; Phillips et al. 1992; Ruiz-Lapuente et al. 1992). The LTE analysis is not self-consistent, since a parameterized temperature distribution is used. The basic procedure of the analysis is to calculate synthetic spectra for a Type Ia supernova explosion model and then compare these spectra with observed spectra. The degree of agreement between the observed and synthetic spectra allows one to make at least a tentative decision about the viability of the explosion model. In some cases, an explosion model can be rejected. Even when the conclusions are less definite, LTE analyses are of great value for making reliable line identifications and extensive explorations of parameter space in order to determine probable features of the supernova ejecta. The discoveries of LTE analyses give immediate guidance for non–LTE (NLTE) analyses and explosion modeling. In making the definitive affirmative decisions on explosion model viability, self-consistent NLTE analyses including relativistic effects are necessary. Such calculations demand considerable computer code development and computer resources. Only recently have

[1] Work based partly on observations at the Multiple Mirror Telescope, a joint facility of the Smithsonian Astrophysical Observatory and the University of Arizona.

[2] Present address: Osservatorio Astrofisico di Asiago, Dipartimento di Astronomia, Università di Padova, Via Osservatorio 8, I-36012 Asiago (VI), Italy.

some modern (although non–self-consistent) NLTE results for the photospheric epoch of Type Ia supernovae become available (Branch et al. 1991; Ruiz-Lapuente et al. 1992). Early NLTE calculations for the photospheric epoch of Type Ia supernovae were done by Feldt (1979, 1980).

Before presenting the analysis and analysis procedure in detail, it is useful to briefly review the standard model of a Type Ia supernovae that has evolved over the last three decades (for full reviews see, e.g., Woosley & Weaver 1986a; Wheeler & Harkness 1990; Woosley 1990). In the standard model, a Type Ia supernova results from the explosion of a white dwarf with mass very near the Chandrasekhar mass of 1.4 $M_\odot$. The white dwarf is usually assumed to consist mainly of carbon and oxygen in nearly equal amounts and to have a uniform composition. The white dwarf is driven to pycnonuclear carbon ignition in its center by the compression and heating caused by accretion of matter either transferred from a red giant companion or from a broken-up white dwarf companion. Because the white dwarf matter is degenerate, the heat released by the burning cannot cause gradual expansion and cooling; heat conduction mechanisms are insufficient to remove heat as quickly as it is produced. The consequence is a thermonuclear runaway that burns the central matter to nuclear statistical equilibrium (NSE). The heat released by burning to NSE relieves the degeneracy, and a burning front or flame is propagated through the star. The inner ~ 0.5–$1\ M_\odot$ of the star is almost entirely burned to iron peak elements (i.e., elements scandium through nickel), with the main constituent being radioactive ^{56}Ni. Since the radioactive ^{56}Ni gives rise to the decay chain $^{56}\mathrm{Ni} \rightarrow {}^{56}\mathrm{Co} \rightarrow {}^{56} \rightarrow \mathrm{Fe}$, the inner region can be called the Ni-Co-Fe core. The half-lives of ^{56}Ni and ^{56}Co are 6.10 and 77.12 days, respectively (Huo et al. 1987). Outside the Ni-Co-Fe core, a substantial amount or all of the remaining matter is burned to intermediate-mass elements. The mechanism for burning front propagation may be deflagration (i.e., turbulent convective subsonic propagation) or deflagration turning into detonation (i.e., a supersonic shock wave that initiates burning) at a transition mass coordinate $M_{\rm tr}$. Models using the latter mechanism are delayed-detonation models (Khokhlov 1991a, b; Woosley 1991) and late-detonation models (Yamaoka et al. 1992); the distinction between the delayed-detonation and late-detonation models has not been completely clarified, but it seems for the delayed case that $M_{\rm tr} \ll 1\ M_\odot$ and for the late case that $M_{\rm tr} \gtrsim 1\ M_\odot$. Pure detonation models burn the entire star to iron peak elements. The presence of significant intermediate-mass elements is, however, required by the observed spectra, and so pure detonation models can be ruled out for Type Ia supernovae. The propagating burning front explodes the star leaving no remnant. The total kinetic energy of the ejecta is $\sim 10^{51}$ ergs. The initial thermal energy of the ejecta becomes unimportant after a few days because of adiabatic cooling. The luminous supernova event that is observed is a result of a reheating of the ejecta by the decay energy released by the ^{56}Ni decay chain. This decay energy, initially in the form of γ-rays and positrons, is mostly degraded into UV/optical/IR radiation during the photospheric epoch.

Various versions of the standard model can explain much of the luminosity and spectral behavior of Type Ia supernovae. The well-known photometric homogeneity (Leibundgut 1988; Leibundgut et al. 1991b) and spectral near-homogeneity (e.g., Filippenko et al. 1992; Phillips et al. 1992) of Type Ia supernovae is explained by the well-defined characteristics of a white dwarf progenitor of nearly the Chandrasekhar mass. The photospheric epoch spectra have been well reproduced in self-consistent LTE calculations (e.g., Harkness 1986, 1991a, b; Wheeler et al. 1986) using the deflagration model W7 of Nomoto, Thielemann, & Yokoi (1984) and Thielemann, Nomoto, & Yokoi (1986). Nebular epoch spectra (Kirshner & Oke 1975), which consists of iron and cobalt emission lines, have been reproduced using a Ni-Co-Fe core model (Axelrod 1980a, b, 1988). The light curves of Type Ia supernovae have been calculated many times with some success using versions of the standard model (e.g., Arnett 1982; Sutherland & Wheeler 1984; Woosley 1990; Harkness 1991b). A recent, fairly successful light-curve calculation using a delayed-detonation model of Khokhlov (1991a, b) has been done by Khokhlov, Müller & Höflich (1992).

Despite its successes, the standard model has some problems. The physics of the explosion is far from being completely solved. Both deflagration and delayed/late-detonation models need to be parameterized to avoid intractable three-dimensional calculations. The initial explosive state of the white dwarf and the history leading to this state are not well understood (see reviews by, e.g., Woosley & Weaver 1986a; Nomoto & Hashimoto 1987; Wheeler & Harkness 1990; Woosley 1990). Given these uncertainties, information about composition and density distribution deduced from spectral analysis is of great benefit in developing the appropriate explosion model. Spectral analysis is most productive when a data set with extensive time and wavelength coverage is available for a supernova, since many constraints are needed to narrow the range of allowed model parameters. Extensive time coverage, for example, allows one to study the composition of the ejecta layers which are progressively revealed by the receding photosphere. Since extensive data sets are available for SN 1990N and SN 1991T, a detailed spectral analysis of these supernovae is well merited.

In § 2 the radiative transfer technique used in the calculations is described. The Type Ia supernovae model used to analyze the spectra is introduced in § 3. The Type Ia supernova photosphere and the photospheric epoch are discussed in terms of this model in § 4. The observations of SN 1990N and SN 1991T and the corrections needed for these observations are discussed in § 5. Sections 6 and 7 report the analyses of SN 1990N and SN 1991T, respectively. In § 8 the synthetic spectra calculated for the analyses and the expanding photosphere method are used for absolute B maximum and distance determinations for the two supernovae. Conclusions and discussion appear in § 9.

2. RADIATIVE TRANSFER TECHNIQUE

The line radiative transfer in the supernova models is calculated using the Sobolev method (e.g., Rybicki & Hummer 1978; Jeffery & Branch 1990). The Sobolev method is appropriate for systems in which the effective velocity width of a line is much smaller than the velocity scale height for changes in the density, temperature, and atomic occupation numbers. For a line for which the Voigt wings and any microturbulent velocity are unimportant, the effective velocity width is just the thermal velocity that gives rise to the line's Doppler profile. Supernova atmospheres have atomic thermal velocities no larger than of order 10 km s^{-1} (except at early and seldom observed epochs), and a lower bound on their velocity scale heights in the photospheric epoch is $\sim 10^3$ km s^{-1}. The ratio of these two velocity scales is $\sim 10^{-2}$. The Sobolev method is probably quite quanti-

tatively accurate for ratios of this size (Hamann 1981; Olson 1982; Natta & Beckwith 1986) and thus is adequate for treating lines in supernova atmospheres. (Note that Hamann's strictures on the Sobolev method's treatment of line blending were made obsolete by Olson.) The Sobolev method formalism used here is not relativistic, but even for the highest detected supernova velocities ($\sim$40,000 km s^{-1}; see § 6.1) the errors introduced by the lack or relativistic effects should be small. A relativistic Sobolev method formalism has been given by Hutsemékers & Surdej (1990).

The line data used for the calculations come from line data files NLTELINES, BELLLIGHT, GFIRONQ, and BELLHEAVY provided by R. L. Kurucz. The opacity calculations done to create these files are described by Kurucz (1991). The files include data on 547,909 lines; 403,107 lines belong to the elements calcium through nickel. Strong lines (or line blends) give rise to P Cygni lines in the spectra of expanding atmospheres. An isolated P Cygni line has a blueshifted absorption and an emission feature centered approximately on the line-center wavelength. The blueshifted absorption is ordinarily formed in matter moving at a velocity equal to or greater than the velocity of the photosphere. The velocity corresponding to the blueshift of the absorption's minimum from the line-center wavelength is called the line velocity; for Type Ia supernovae in the photospheric epoch line velocities are of order 10,000 km s^{-1}. Because of line blending and NLTE effects, there are only a few relatively clean P Cygni lines in a spectrum. In the distortion of P Cygni lines by line blending and NLTE effects, it turns out that the absorption is usually much more robust and identifiable than the emission feature, and therefore it is the absorption that is usually labeled; this practice is followed in this paper (see §§ 6 and 7). An extensive discussion of P Cygni line formation in supernova atmospheres is given by Jeffery & Branch (1990).

The continuous opacity situation of supernova atmospheres is complicated by the presence of electron scattering, bound-free, free-free, and expansion opacities. The electron scattering opacity, which is, of course, a wavelength-independent opacity, is responsible for the electron photosphere of a supernova (see § 4). The bound-free and free-free opacities are essential for self-consistent calculations, since they couple the radiation field to the local electron temperature. However, they are considerably smaller than the electron scattering and expansion opacity in the UV (down to $\sim$1000 Å) and optical of Type Ia supernovae (e.g., Harkness 1991b, Fig. 2), and thus their direct effect on the flux transfer in these wavelength regions is small. For the present analysis, a self-consistent calculation for temperature was not attempted, and thus the coupling effect of the bound-free and free-free opacities was not needed. Since the direct effect of the bound-free and free-free opacities is small, they were not included in the calculations. The temperature distribution assumed for the calculations is described in § 3.

The expansion opacity (Karp et al. 1977) is the quasi-continuous opacity due to lines so densely packed in wavelength and that the wavelength intervals in which they have significant opacity are heavily overlapped; such densely packed lines can be called "overlapping" lines for convenience. The name "expansion opacity" is due to the fact that the opacity wavelength intervals, and hence the overlapping, are greatly increased by large expansion velocities such as exist in supernova atmospheres. This spreading out of the line opacity due to expansion can sometimes greatly decrease the saturation of the line opacity, and thus can greatly increase the line opacity's effect on the overall radiation transport in the atmosphere. A single line or line blend cannot form a P Cygni line unless its opacity is sufficiently larger than the average line opacity in its spectral region. The expansion opacity in Type Ia supernova atmospheres is dominant in the region $\sim$1000–4000 Å and is very large in the region $\sim$300–3000 Å (e.g., Harkness 1991b, Fig. 2). In these regions the expansion opacity is mainly due to lines of iron peak elements. The expansion opacity is responsible for the ultraviolet deficiency of a Type Ia supernova spectrum relative to a Planck curve fitted to the optical region (Wheeler et al. 1986; Harkness 1991b). Only extremely strong lines blueward of 4000 Å, the Ca II H and K lines being the clearest examples, can form obvious P Cygni lines. Flux peaks blueward of the Ca II H and K P Cygni emission feature are usually better thought of as due to relative gaps in the expansion opacity's line blanketing than due to P Cygni emission features. The expansion opacity redward of 4000 Å is weaker than the electron opacity and is formed chiefly by weak lines. Since the net contribution of many weak lines to the expansion opacity is significant, all lines from the Kurucz files belonging to the relevant elements in the relevant wavelength regions have been included in the calculations.

In order to treat the continuum and line radiative transfer in a unified manner in a Sobolev method calculation, the electron and line opacities in a specified wavelength interval (see below) are treated as the opacity due to a single pseudoline. The wavelength of the pseudoline is the opacity-weighted average wavelength of the wavelength interval. The electron opacity becomes the electron part of the pseudoline and the true line opacity, the line part of the pseudoline. The source function for the electron part of the pseudoline is a scattering source function with angular redistribution determined by the Rayleigh phase function; treatment of photon angular redistribution with the Rayleigh phase function requires the use of a modified Sobolev formalism, the Sobolev-P method (Jeffery 1988, 1989, 1990). The electron part of the pseudoline conserves energy. The line part of the pseudoline is given an LTE source function: i.e., the Planck function evaluated with the assumed local temperature and the pseudoline's wavelength. With this line part source function, photons absorbed by the line part are thought of as being converted into local thermal energy; i.e., the true lines are considered to be pure absorption lines. The line part could have been given a scattering source function, in which case the pseudoline would have become a pure scattering line. For a line, the LTE and scattering source functions are two limiting approximations; the true source function behavior does not, however, necessarily lie between these two approximations and has to be determined from self-consistent NLTE calculations. The LTE source function was chosen for the line part because it gave better fits to the observed spectra than did the scattering source function.

The pseudoline treatment of the opacity and source function is approximate on several counts. First, compacting all the opacity for a wavelength interval into a single wavelength increases the overall saturation of the opacity and thus decreases the net effect of the opacity on the radiation transport. This spurious effect can be reduced to a tolerable level by decreasing the wavelength intervals of pseudolines. The prescription used for the wavelength interval is

$$\Delta\lambda = h \frac{v_{\rm char}}{c} \lambda , \qquad (1)$$

where v_{char} is a characteristic line velocity and h is an adjustable parameter. With the computer code used for the present work, the computing time for synthetic spectrum increased more rapidly than linearly with h^{-1}. Experience shows that a synthetic spectrum is usually constant as h is varied (i.e., the spurious saturation effect has usually disappeared) when $h \leq 0.1$. A second limitation of the pseudoline treatment is that line opacity is shifted from its true wavelength position to the average wavelength. Because of the small size of wavelength interval (when $h \lesssim 0.1$) compared with the Type Ia supernova P Cygni line width [$\gtrsim (v_{char}/c)\lambda$], the artificial wavelength shifts are not a significant error. The shifting error can also be reduced by decreasing h. In calculations for synthetic spectra shown in §§ 6 and 7, h-values of 0.05 or 0.1 were used.

Another limitation of the pseudoline treatment is the joint treatment of line and electron opacities. For the lines alone with the assumption that they are acting as pure absorption lines, the Sobolev method should be reasonably adequate provided that the effective velocity width of the line is less than of order 10^3 km s^{-1} which is the velocity interval over which it can be assumed that physical variables such as density, temperature, and atomic occupation numbers are roughly constant. One would expect only lines with Sobolev optical depths of order 10^4 or larger to be in danger (because of significant opacity in their Voigt wings) of violating this effective velocity width criterion. Lines of this strength were encountered in the calculations in only a few cases in UV regions where the lines are so heavily overlapped that individual line behavior is totally washed out and exact treatment for any one line, even a strong one, seems unnecessary. If it is not assumed that the lines act as pure absorption lines, then the complications of line photon redistribution may need to be considered for such strong lines. For the electron scattering opacity alone, it has been shown (Jeffery 1989, 1991b) that the pseudoline treatment is quantitatively accurate at least for electron opacity optical depths of order 10 or less. For the calculations reported here, the electron opacity optical depth to the lower boundary of the model was always less than 2. The question remains whether the combined treatment of the electron scattering and line opacities introduces some systematic error. Since the pseudoline treatment should be reasonably accurate for the extremes of pure line or pure electron scattering opacity, it is plausible that the treatment interpolates to a reasonable accuracy for intermediate situations; in any case, much of the time a pseudoline's behavior is dominated by one of the two forms of opacity.

3. THE TYPE Ia SUPERNOVA MODEL

For the calculation of synthetic spectra, one can either use a model supernova calculated from a hydrodynamic explosion with nucleosynthesis or a schematic model based on theoretical ideas and observational constraints. The former approach can be too restrictive, since the available calculated models may not fit all the available constraints very well. On the other hand, it is difficult to construct a schematic model in sufficient realistic detail; for example, it is not simple to create a parameterized complex stratified composition. For the current research, a compromise between the two approaches was adopted in order to have the freedom to adjust some model parameters and still have realistic detail in the model.

The model that has been adopted is spherically symmetric and has an exponential density profile as function of ejecta velocity:

$$\rho = \rho_0 \exp(-v/v_0), \quad (2)$$

where ρ_0 is the central density and v_0 is the e-folding velocity. (Within tens of seconds after the ignition of the explosion in the exploding white dwarf scenario, a Type Ia supernova enters a state of [uniform motion] homologous expansion [e.g., Jeffery & Sutherland 1985]. The initial radii of matter elements in the ejecta become negligible within a similar time. Thus, the velocity of a matter shell becomes an appropriate comoving coordinate for describing the ejecta. The radius and velocity coordinates are related by $r = vt$, where t is the time since the ignition of the explosion.) The exponential density profile was adopted because both deflagration and delayed/late-detonation explosions can yield density profiles that are roughly exponential. The well-known deflagration model W7 of Nomoto et al. (1984) has a density profile that is roughly exponential with an e-folding velocity of $\sim$2400 km s^{-1} up to about 21,000 km s^{-1}; above this velocity, the density profile falls below an exponential and the model has a cutoff at 22,027 km s^{-1}; the burned region of the model W7 ends at $\sim$14,900 km s^{-1}. The delayed-detonation model DD2 of Woosley (1991) has an even more exponential-like density profile than that of model W7. It has an approximate e-folding velocity of $\sim$3160 km s^{-1}, ejecta moving at least as fast as 31,000 km s^{-1}, and a burned region extending to $\sim$29,000 km s^{-1}. The exponential nature of the late-detonation model density profiles is known from a private communication (Thielemann 1992). Since SN 1990N gives evidence for ejecta moving as fast as $\sim$40,000 km s^{-1} and burned material as fast as $\sim$25,000 km s^{-1} (see § 6.1), a very extended density profile like that of model DD2 seemed appropriate for the present paper. Thus, for all the calculations, the exponential density profile was given an e-folding velocity of 3160 km s^{-1}. The total mass of the model was set to the Chandrasekhar mass of 1.4 $M_\odot$. The total kinetic energy is then

$$E = 6Mv_0^2 = 1.67 \times 10^{51} \text{ ergs}. \quad (3)$$

This kinetic energy is 30% greater than that of model W7 and may be nearly as large as can be obtained from a plausible deflagration explosion in a C-O white dwarf with a mass near the Chandrasekhar mass (e.g. Woosley 1990).

Because supernovae (after early times) are in homologous expansion, the density at all velocities is proportional to t^{-3}. Thus, given t, the density of the model at all points is determined. For a model with an exponential density profile, the expression for the central density as a function of time is

$$\rho_0 = \frac{M}{8\pi v_0^3 t^3}, \quad (4)$$

where M is the total mass of the model. The explosion of a Type Ia supernova has never been observed, and thus t has never been known exactly. Leibundgut et al. (1991a) have estimated that the B maximum for SN 1990N is 20 days after the explosion; this estimate has an uncertainty of at least 2 days. For the present analysis, t is calculated in all cases assuming 20 days as the rise time to the B maximum (i.e., as the time from the explosion to the maximum light epoch).

The stratified compositions of deflagration and delayed detonation explosion models are qualitatively very similar, although quantitative differences can be significant (Nomoto et al. 1984; Thielemann et al. 1986; Woosley 1991; Khokhlov 1991b). As mentioned in § 1, there is a Ni-Co-Fe core. Above this core is a layer dominated by (in order of abundance) silicon, sulfur, calcium, and argon: the latter two might have

their positions interchanged. Above this layer is a layer dominated by oxygen and magnesium. In the deflagration model W7, the subsonic burning front is turned off by the low density in the outer white dwarf caused by expansion ahead of the front, and thus an outer layer of unburned carbon-oxygen composition is left. In the delayed-detonation models the oxygen-magnesium–dominated layer extends to the surface, since the detonation burning front (which started deep in the interior of the white dwarf, where it produced part of the Ni-Co-Fe core) continues to the surface (Khokhlov 1991b). The late-detonation models are somewhat different; in their case, the late detonation starts after a layer of intermediate-mass elements has been formed by deflagration. Above this intermediate-mass element layer, the late detonation creates a layer rich in iron peak and silicon peak elements, with a second layer of lower mass intermediate-mass elements still farther out (Yamaoka et al. 1992).

For the present work the revised W7 composition of Thielemann et al. (1986) was adopted as a starting composition, and modifications were made in order to fit the observed spectra. The procedure for determining the modifications was rough and nonrigorous; plausible modifications were tried and were adopted if they improved the fit to the observations. Stratified compositions have too many parameters for a rigorous procedure for a best fit to be easily done. The compositions (as they appear at $t = 0$) that were finally adopted for synthetic spectrum calculations for SN 1990N and SN 1991T are displayed in §§ 6 and 7, respectively.

As mentioned in § 1, the LTE analysis reported here is not self-consistent, since a calculation for temperature is not done. The development of the computer code and data files of bound-free and free-free opacities needed for a self-consistent LTE solution was beyond the scope of the present research. Instead of solving for temperature, the temperature law of the static, radiative equilibrium, spherical, gray (i.e., wavelength-independent opacity) atmosphere has been assumed for the model. A derivation of the form of this law used here can be given; Mihalas (1978, pp. 245–246) gives a derivation of the law for atmospheres where the opacity is proportional to an inverse power of radius. If it is assumed that the (gray) opacity is proportional to density, then the opacity obeys

$$\kappa = C \exp(-r/r_0), \tag{5}$$

where C is a constant and $r_0 = v_0 t$ is the e-folding distance. The optical depth is given by

$$\tau(r) = C r_0 \exp(-r/r_0) \tag{6}$$

and the differential optical depth by

$$d\tau = -C \exp(-r/r_0) dr . \tag{7}$$

From Mihalas (1978, p. 245), the wavelength-integrated mean intensity for a spherical gray atmosphere is

$$J(r) = 3H_0 \int_0^{\tau(r)} \frac{d\tau'}{r'^2} \quad \text{for} \quad \tau(r) \gg 1 , \tag{8}$$

where $H_0 = L/(16\pi^2)$; L is the luminosity of the atmosphere. With the exponential opacity law,

$$J(r) = 3H_0 C \int_r^R \frac{\exp(-r'/r_0)}{r'^2} dr' \quad \text{for} \quad r \ll R , \tag{9}$$

where R is the outer radius of the atmosphere. If $R \to \infty$ and the transformation $r' = rx$ is introduced, then

$$J(r) = \frac{3H_0 C}{r} \int_1^\infty \frac{\exp(-xr/r_0)}{x^2} dx = \frac{3H_0 C}{r} E_2(r/r_0) , \tag{10}$$

where $E_2(x)$ is the second exponential integral. For $r \gg r_0$,

$$J(r) = \frac{3H_0 C}{r} \frac{\exp(-r/r_0)}{r/r_0} = \frac{3H_0 \tau(r)}{r^2} . \tag{11}$$

For $\tau \ll 1$ (i.e., the free-flow regime),

$$J(r) = \frac{H_0[\tau(r) + 1]}{r^2} \tag{12}$$

(e.g., Mihalas 1978, p. 246). The interpolation formula obtained for equations (11) and (12) is

$$J(r) = \frac{H_0[3\tau(r) + 1]}{r^2} = \frac{L[3\tau(r) + 1]}{16\pi^2 r^2} . \tag{13}$$

Making the LTE assumption gives

$$J(r) = B[T(r)] = \frac{\sigma_r T^4}{\pi} , \tag{14}$$

where $B(T)$ is the wavelength-integrated Planck function and $\sigma_r = 5.67 \times 10^{-5}$ ergs cm^{-2} K^{-4} s^{-1} is the Stefan-Boltzmann constant. Finally, an expression for temperature in terms of a reference temperature T_1 at optical depth τ_1 is obtained:

$$T = T_1 \left[\left(\frac{r}{r_1} \right)^{-2} \left(\frac{\tau + 1/3}{\tau_1 + 1/3} \right) \right]^{1/4} . \tag{15}$$

Equation (15) for the gray atmosphere temperature profile was the expression used in the present work. It is plausible temperature profile that certainly incorporates some of the right physical effects. It has, however, several limitations: (1) It is only an interpolation formula for a gray atmosphere, and supernova atmospheres are not gray. (2) It is for a static atmosphere, and it has been shown that corrections to static atmosphere temperature profiles for flows with supernova-like velocities are not always negligible (Hauschildt, Best, & Wehrse 1991). (3) The assumption of LTE is not exactly correct; corrections to LTE ionization and excitation predictions can be a factor of 3 or much more (e.g., Branch et al. 1991). (4) Because of the energy deposition from the decay of the radioactive isotopes, Type Ia supernova atmospheres are not in radiative equilibrium (e.g., Ambwani & Sutherland 1988). Most of the deposition is in the interior of the ejecta, where the bulk of the radioactive isotopes are located; thus, to some approximation radiative equilibrium does apply for the photospheric epoch (see definition below). Thermal energy left in the atmosphere from the explosion would also violate radiative equilibrium; this energy, however, is probably negligible a few days after the explosion. (5) To use equation (15), the most appropriate optical depth scale would be the Rosseland mean optical depth scale. At great depths (but still with $r \gg r_0$) in a static, radiative equilibrium atmosphere with an exponential Rosseland mean opacity profile and with a known luminosity to fix T_1 at $\tau_1 \gg 1$, equation (15) with a Rosseland mean optical depth argument would give the correct temperature (e.g., Mihalas 1978, pp. 58, 245). Unfortunately, the real

Rosseland mean opacities can only be obtained from a self-consistent calculation and so are unavailable here. Instead of using the Rosseland mean optical depth scale, a characteristic exponential optical depth scale is assumed that has $\tau_1 = 1$ at a velocity $v_1 = r_1/t$ that is characteristic of line formation. Both v_1 and the temperature T_1 were used as parameters for fitting the observed spectra.

For the calculations, the inner boundary radiation field at the characteristic optical depth τ_2 was given by the diffusion approximation

$$I_\lambda(\tau_2, \mu) = B_\lambda(\tau_2) + \mu\left(\frac{dB_\lambda}{d\tau}\right)\bigg|_{\tau_2} \quad \text{for} \quad \mu \geq 0\,, \tag{16}$$

where $I_\lambda(\tau, \mu)$ is the specific intensity, μ is the cosine of the angle to the radius, and $B_\lambda(\tau)$ is the Planck function as a function of τ (e.g., Mihalas 1978, p. 51). The inner boundary optical depth τ_2 was chosen to be sufficiently large that a calculated synthetic spectrum remained fairly constant as τ_2 was increased. However, complete insensitivity to the location of the inner boundary was not achieved in all cases, and thus the inner boundary location becomes a significant parameter of the model. In §§ 6 and 7, the inner boundary velocity v_2 and temperature T_2 are specified for each calculation. To calculate the derivative in equation (16), the derivative of equation (15) is needed:

$$\frac{dT}{d\tau} = T_1\left[\frac{1}{2}\left(\frac{r}{r_1}\right)^{-3/2}\frac{r_0}{r_1\tau}\left(\frac{\tau + 1/3}{\tau_1 + 1/3}\right)^{1/4} + \left(\frac{r}{r_1}\right)^{-1/2}\left(\frac{\tau + 1/3}{\tau_1 + 1/3}\right)^{-3/4}\left(\frac{1/4}{\tau_1 + 1/3}\right)\right]. \tag{17}$$

The temperatures obtained from the gray atmosphere temperature profile may have errors of order 2000 or 3000 K just from the uncertainty in the fit to the spectrum. Errors of this size can result in order-of-magnitude errors in abundance estimates. The reason for this is that most of the lines seen in Type Ia supernova spectra belong to singly ionized atoms, but at temperatures of order 10,000 K (which is, very roughly, the characteristic atmosphere temperature in the photospheric epoch of Type Ia supernovae) most of the atoms are doubly ionized. Most of the lines of the doubly ionized atoms are too far in the UV or have excitation energies that are too high for them to cause features in the observed spectra. The abundances of the singly ionized species are often lower by orders of magnitude than those of the doubly ionized species, and thus can be very sensitive to temperature. A change in temperature of order 10^3 K can change the abundance of a singly ionized species by an order of magnitude. The situation is not quite so bad as it seems, since relative abundance determinations of elements with similar ionization energies made on the basis of their singly ionized abundances probably have smaller uncertainties than absolute abundance determinations made on the same basis would have. Nevertheless, an order-of-magnitude uncertainty at least must be assumed for any element abundance determination, absolute or relative, made using the gray atmosphere temperature profile. Since NLTE effects can also lead to errors of an order of magnitude or more in ionization fraction determinations for a given temperature (e.g., Branch et al. 1991), abundance determinations made in this paper must be regarded as only suggestive. Suggestive determinations, however, are of considerable value in the absence of more decisive determinations.

4. THE TYPE Ia SUPERNOVA PHOTOSPHERE AND PHOTOSPHERIC EPOCH

There are various definitions of "photosphere" in the supernova literature. A reasonable definition is that the photosphere is that shell in the atmosphere from which a radially outward-directed photon has a 50% chance of escaping the atmosphere without interacting again with continuous opacity. The probability of escape from a given point in a given direction is $\exp(-\tau)$, where τ is the continuum optical depth from the point to infinity. For a 50% chance of escape, $\tau = \ln 2 = 0.6931$. This continuum optical depth value is conveniently close to $\frac{2}{3}$, which is the continuum optical depth to the point in an LTE plane-parallel gray atmosphere where temperature equals the effective temperature in the Eddington approximation (e.g., Mihalas 1978, p. 61). For expanding spherical atmospheres, the continuum optical depth along the line of sight through the center of the atmosphere to the place where the absorptions of weak P Cygni lines form is also of order $\frac{2}{3}$ (e.g., Eastman & Kirshner 1989); at deeper points in the atmosphere the continuous opacity is strong enough to largely wash out weak line effects. Thus, from several points of view, defining the photosphere to be at continuum optical depth $\frac{2}{3}$ in the atmosphere is sensible. For Type Ia supernovae this definition has two deficiencies. First, because of the strong expansion opacity, the photosphere in the UV region will be much nearer the surface than in the optical, where electron scattering opacity is dominant. Second, because of composition stratification, weak line absorptions can form above the photosphere. The most striking case of this occurs when the photosphere recedes into the Ni-Co-Fe core of the Type Ia supernova ejecta. When this happens, the absorptions of lines of the intermediate-mass elements must form above the photosphere. In order to be definite, the photosphere definition adopted in this paper is that the photosphere is at electron scattering optical depth $\frac{2}{3}$. The photospheric epoch is defined as that time from the explosion until the photosphere recedes to the center of the ejecta. The period after the photospheric epoch is called the "nebular epoch."

Spectrophotometry of Type Ia supernovae shows that the bulk of the radiation energy in the UV/optical/IR region emerges in the optical, where electron scattering is the dominant form of continuous opacity during the photospheric epoch. Thus, the electron scattering opacity is a "valve" that releases stored energy of which the ultimate source is deposition from the radioactive elements in the Ni-Co-Fe core. One would expect that there would be a change in photometric behavior when the "valve" is completely opened at the end of the photospheric epoch. This change in behavior is probably the rather sharp transition of the *UBV* light curves at about 30 days after the maximum light from steeply declining to a slower exponential decline (e.g., Leibundgut et al. 1991b).

It is possible to make an approximate prediction of the end of the photospheric epoch using the model introduced in § 3. If it is assumed that the electron density is everywhere proportional to the density and so declines exponentially with e-folding velocity v_0, then the electron opacity optical depth to a velocity v is given by

$$\tau_e = \frac{\rho_0}{\mu_e m_u}\sigma_e v_0 t \exp\left(\frac{-v}{v_0}\right), \tag{18}$$

where μ_e is the mean molecular weight per electron (e.g., Clayton 1983, p. 84), $m_u = 1.66 \times 10^{-24}$ g is the atomic mass

unit, and $\sigma_e = 6.65 \times 10^{-25}$ cm^{-2} is the Thomson cross section. Using equations (4) and (18), one finds that the time from the explosion until the photosphere recedes to velocity v is given by

$$t = \left(\frac{M\sigma_e}{8\pi\tau_e \mu_e m_u}\right)^{1/2} \frac{\exp(-v/2v_0)}{v_0}$$
$$= 56.5\left[\left(\frac{M}{1.4\ M_\odot}\right)\left(\frac{28}{\mu_e}\right)\left(\frac{2/3}{\tau_e}\right)\right]^{1/2}$$
$$\times\left(\frac{3160\ \text{km s}^{-1}}{v_0}\right)\exp\left(\frac{-v}{2v_0}\right)\text{days}. \quad (19)$$

If $M = 1.4\ M_\odot$, $\mu_e = 28$ (appropriate for material dominated by doubly ionized iron peak species of atomic mass 56), $\tau_e = \frac{2}{3}$, and $v_0 = 3160$ km s^{-1}, the predicted end of the photospheric epoch (i.e., when $v = 0$) occurs at about day 56.5 after the explosion. This prediction is roughly in agreement with the time when the light curves enter the exponential decline phase (still assuming that maximum light occurs at about day 20), and thus tends to confirm the expectation of a close connection between the end of the photospheric epoch and the change in the light-curve behavior. In model W7 the Ni-Co-Fe core boundary is at about 9000 km s^{-1}. Using this velocity for v, $\mu_e = 14$ (appropriate for doubly ionized silicon–dominated material), and the other parameters as before, equation (19) predicts day 19.2 as the time when the photosphere is at the core boundary. Thus, after about maximum light, one would expect in the case of model W7 that the lines of the intermediate-mass elements would no longer be "photospheric"; i.e., these lines will form above the photosphere because it has receded below the layers with significant intermediate-mass element abundance.

5. THE OBSERVATIONS OF SN 1990N AND SN 1991T

SN 1990N occurred in NGC 4639 and had a B maximum (corrected for foreground Galactic extinction) of 12.65 mag on 1990 July 10.5 UT (Leibundgut et al. 1991a). It appears to have been a typical Type Ia supernova. It is remarkable, however, in that it has the earliest observed optical and *IUE* UV spectra and, with the exception of Type Ia supernova SN 1992A (Kirshner et al. 1992), the most complete set of *IUE* UV spectra available for a Type Ia supernova. The earliest optical and UV spectra were obtained 14 days before maximum light (i.e., before the B maximum epoch). This unique data set makes SN 1990N a most valuable supernova for intensive theoretical study.

SN 1991T occurred in NGC 4527 and had a B maximum (corrected for foreground Galactic extinction) of 11.64 ± 0.05 mag on 1991 April 28.5 UT (Phillips et al. 1992). This supernova has spectra from 12 days before maximum light and has been well observed since its discovery. Its premaximum spectra are qualitatively unlike those of SN 1990N or the other Type Ia supernovae observed well before maximum light, as pointed out by Filippenko et al. (1992). The premaximum spectra of these other Type Ia supernovae (SN 1971I [Kikuchi 1971], SN 1974G [Iye et al. 1975], SN 1975A [Kirshner, Arp, & Dunlap 1976], SN 1984A [Wegner & McMahan 1987; Branch 1987; Barbon, Iijima, & Rosino 1989], SN 1986G [Phillips et al. 1987], and SN 1989B [Barbon et al. 1990; Phillips et al. 1992]) are recognizably similar to those of SN 1990N. After maximum light, the SN 1991T spectra became similar to those of other Type Ia supernovae (Filippenko et al. 1992; Phillips et al. 1992). Up to maximum light, the SN 1991T B and V light curves gave a close fit to the template light curves derived from well-observed Type Ia supernovae; after maximum light, the B and V light curves showed a slightly slower decline than that given by the template light curves (Phillips et al. 1992). The template light curves (Leibundgut 1988; Leibundgut & Tammann 1992) seem to fit many other Type Ia supernova light curves to within observational uncertainty (Leibundgut et al. 1991b). The peculiarities of SN 1991T make it an important object to consider when evaluating the use of Type Ia supernovae as standard candles and, of course, have implications for Type Ia supernova models. One of the aims of this paper is to study the differences between SN 1990N and SN 1991T and decide whether these supernovae arise from similar explosions with superficial differences or from fundamentally different explosions.

Table 1 lists the spectra used for the analyses. The spectra for different, but close, epochs have been combined in some cases in order to give a spectrum with broad wavelength coverage; the combinations used are introduced in §§ 6 and 7. Supernova spectra after the usual instrumental reductions require, in general, a correction for the redshift of the parent galaxy, corrections for foreground Galactic extinction and parent galaxy extinction, and a correction to give the spectra photometric accuracy. The corrections undertaken for the spectra used here are detailed below.

The parent galaxy redshifts of observed spectra were corrected using the heliocentric velocities 975 ± 10 km s^{-1} for NGC 4639 and 1735 ± 10 km s^{-1} for NGC 4527 (Huchtmeier & Richter 1989). The interstellar Na I D lines (Smith & Wheeler 1991) and Ca II H and K lines (Meyer & Roth 1991) in the SN 1991T spectra due to the parent galaxy NGC 4527 exhibit at least three components, showing that there are at least three intervening interstellar clouds in NGC 4527. The velocities of these clouds range between 1764 and 1807 km s^{-1}. Because the clouds need not have velocities that are closely related to the velocity of the supernova, there is no reason to prefer the cloud velocities to the parent galaxy velocity for correcting the redshifts of the SN 1991T spectra. In any case, velocity differences of ~ 100 km s^{-1} or less would cause shifts of order 3 Å or less in the observed spectra, and so are unimportant for spectrum analysis. Since parent galactic rotational velocities are of order 100 km s^{-1}, they can be neglected as well for both supernovae.

The foreground Galactic $E(B-V)$ values for SN 1990N and SN 1991T from the tables of Burstein & Heiles (1984) are 0.012 and 0.000 mag, respectively. The spectra shown in §§ 6 and 7 have been corrected using these values and the extinction law of Cardelli, Clayton, & Mathis (1989) with $R_V = 3.1$ (the standard value for the diffuse interstellar medium). Hereafter, the Cardelli et al. extinction law with $R_V = 3.1$ will be called the conventional extinction law. The extinctions in the parent galaxies NGC 4639 (SN 1990N) and NGC 4527 (SN 1991T) are difficult to estimate. Since SN 1990N has no strong interstellar absorption lines (Leibundgut et al. 1991a), its extinction is probably small and has been assumed to be zero in this paper. Filippenko et al. (1992) and Ruiz-Lapuente et al. (1992) estimate $E(B-V)$ values of ~ 0.2 and 0.34 mag, respectively, for SN 1991T based on interstellar Na I D lines in the parent galaxy. Such estimates are quite uncertain. If the assumption is made that SN 1991T had normal Type Ia supernova brightness, then an upper limit on extinction can be placed. The mean B maximum of Virgo Cluster Type Ia supernovae is

TABLE 1

SPECTRA OF SN 1990N AND SN 1991T

Date (UT)	Spectral Range (Å)	Epoch Relative to Maximum Light (days)	Epoch Relative to Explosion (days)	Observatory	Reference or Observer
		SN 1990N			
1990 Jun 26.2	3200–8400	−14.3	5.7	MMT	Leibundgut et al. 1991a
1990 Jun 26.8	1700–3200	−13.7	6.6	*IUE*	Leibundgut et al. 1991a
1990 Jul 2.7	1700–3250	−7.8	12.2	*IUE*	Leibundgut et al. 1991a
1990 Jul 3.0	3250–7700	−7.5	12.5	CTIO	Leibundgut et al. 1991a
1990 Jul 14.1	1700–3300	3.6	23.6	*IUE*	Leibundgut et al. 1991a
1990 Jul 17	3900–9900	~7	~27	Lick	Leibundgut et al. 1991a
		SN 1991T			
1991 Apr 18.2	3200–5800	−10.3	9.7	MMT	C. B. Foltz
1991 Apr 19.2	4850–10100	−9.3	10.7	MMT	C. B. Foltz
1991 Apr 25.0	3050–10400	−3.5	16.5	CTIO	Phillips et al. 1992
1991 Apr 29	1700–3400	1.2	21.2	*IUE*	G. Sonneborn
1991 May 8–8	3150–10200	~11	~31	CTIO	Phillips et al. 1992

NOTE.—It has been assumed that a Type Ia supernova explosion occurs 20 days before maximum light (see § 3). MMT is the Multiple Mirror Telescope on Mount Hopkins, *IUE* is the *International Ultraviolet Explorer* satellite, and CTIO is the Cerro Tololo Inter-American Observatory.

11.9 ± 0.2 mag (Leibundgut & Tammann 1990). Since Tully-Fisher determinations of the relative distance modulus between NGC 4527 and the Virgo Cluster give -0.4 ± 0.2 mag (derived from Pierce & Tully 1988 and Tully, Shaya, & Pierce 1992) and -0.7 ± 0.4 mag (derived from Peletier & Willner 1991), a value for this relative distance modulus of -0.6 ± 0.5 mag has been adopted here. Consequently, assuming the Virgo Type Ia supernovae give the true unextinguished Type Ia supernova B maximum distribution, the predicted NGC 4527 Type Ia supernova B maximum would be 11.3 ± 0.7 mag. The observed SN 1991T B maximum of 11.64 ± 0.05 mag is consistent with the prediction within uncertainty, and thus SN 1991T could have suffered negligible extinction. The large size of the uncertainty in the prediction means, however, that the upper limit on extinction is ~1 mag in B. There is, however, an argument for extinction significantly lower than 1 mag for SN 1991T.

The argument for low extinction is based on the strong shape similarity (not considering line profiles) in the optical and near-IR (optical/NIR) of all the premaximum spectra of both SN 1990N and SN 1991T. This similarity can be shown by overlaying all these spectra (corrected for foreground Galactic extinction, for parent galaxy redshift, and to obtain photometric accuracy [see below]) and forcing them to have the same net flux in the wavelength range 4500–7500 Å. Figure 1 shows such an overlay, which for clearness has only the earliest available premaximum spectrum of SN 1990N and the latest available premaximum spectrum of SN 1991T; using spectra from different epochs emphasizes the time-independence of the similarity. In addition to the optical/NIR shape similarity, there is some shape similarity blueward of 4000 Å. The similarity of the premaximum spectra suggests both intrinsic similarity of the two supernovae and that there is little difference in reddening between them. Quantitatively, one asks how much difference between the supernovae and their respective reddenings is plausible. To investigate this, blackbody curves have been fitted to the optical/NIR of the April 25 SN 1991T spectrum by forcing the net flux in the range 5500–10000 Å of the spectrum and curves to be the same (see Fig. 1). The optical/NIR continuum flux of the supernovae must actually form in a layer with some range of temperature and will also suffer varying degrees of blueshift due to the expansion of the ejecta; the latter effect decreases the mean slope (i.e., increases the absolute value of the mean slope) of a blackbody curve between 4000 and 10000 Å by less than 5% at 10,000 K, and the effect decreases with increasing temperature. Because of these complications, the optical/NIR continuum flux will be a distorted blackbody flux. For simplicity, however, the assumption is made that the optical/NIR continuum flux-forming layer approximates a blackbody radiator. With this assumption and the assumption of no parent galaxy reddening, the blackbody curves in Figure 1 show that the optical/NIR color temperatures of the supernovae are probably in the range ~12,000–20,000 K. With some understanding of P Cygni line formation in the supernovae (see §§ 6 and 7), a judgment can be made that $14{,}000 \pm 2000$ K is the best color temperature for both supernovae. To see the effect of reddening on these conclusions, a 30,000 K blackbody curve reddened using $E(B-V) = 0.3$ mag and the conventional extinction law has also been fitted (just as the unreddened blackbody curves were) to the April 25 spectrum of SN 1991T (see Fig. 1). This reddened curve is only a marginally good fit. Given the good agreement between the supernovae's spectra, a large intrinsic color temperature difference and a large canceling reddening difference seem too coincidental. Moreover, in the spectrum analyses of the premaximum spectra given in §§ 6 and 7, no need was found for excitation or radiation field temperatures higher than 16,000 K. Thus, an $E(B-V)$ difference between the two supernovae as large as 0.3 mag is ruled out. In a similar manner, but more tentatively, an $E(B-V)$ difference as large as 0.2 mag is ruled out. An $E(B-V)$ difference as large as 0.1 mag cannot be ruled out, but is slightly disfavored. If the conventional extinction law (with $R_B = 4$) is valid for SN 1991T, then the small reddening difference between the two supernovae also implies a B-band extinction difference that is probably less than 0.8 mag and perhaps less than 0.4 mag. There is some evidence that the extinction laws that apply for Type Ia supernovae may often decline more steeply with wavelength than

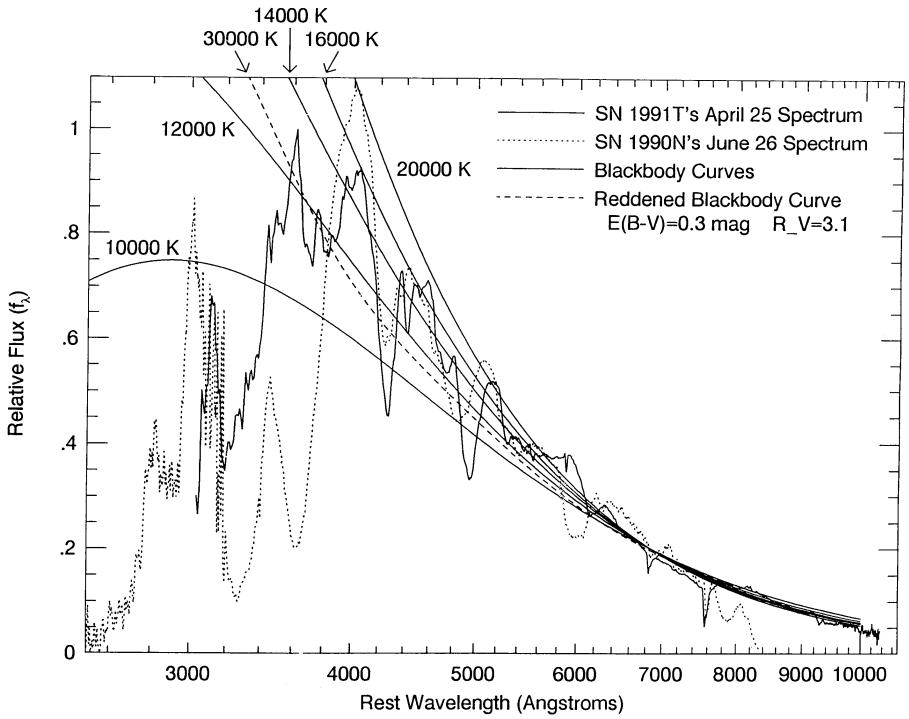

FIG. 1.—Overlay of the June 26 spectrum of SN 1990N and the April 25 spectrum of SN 1991T. Blackbody curves and a reddened blackbody curve show possible fits to the optical and near-IR flux continuum of the two supernova spectra.

the conventional extinction law and have $R_B \lesssim 2$ (Jöeveer 1982; Capaccioli et al. 1990; Branch & Tammann 1992; Leibundgut & Tammann 1992; pace Della Valle 1991; Della Valle & Panagia 1992). If $R_B \lesssim 2$ applies for SN 1991T, then the extinction difference between SN 1991T and SN 1990N is probably less than 0.4 mag and perhaps less than 0.2 mag. Given these arguments for a relatively low extinction difference between SN 1990N and SN 1991T, it has been assumed that the parent galaxy extinction for SN 1991T is zero also.

In § 6, optical and *IUE* UV spectra are combined for SN 1990N. The *IUE* spectra are probably accurate in absolute flux to about 10%. The optical spectra obtained with narrow slits in variable seeing are not necessarily so accurate, and thus photometric correction factors for these spectra need to be calculated. The factors were calculated from the difference between spectrum-derived magnitudes and photometric magnitudes for the epochs of the spectra. Spectrum-derived *B* and *V* magnitudes were obtained from the observed optical spectra using the response curves and Vega zero-point magnitudes recommended by Bessell (1990) and the favored synthetic Vega spectrum of Dreiling & Bell (1980). Photometric *B* and *V* magnitudes were calculated for the epochs of the spectra from the Type Ia supernova template *B* and *V* light curves fitted to the observed *B* and *V* light curves of SN 1990N (Leibundgut et al. 1991a). The scatter of the observed *B* and *V* magnitudes about the template light-curve fits is less than about 0.1 mag (Leibundgut et al. 1991a), and thus the calculated photometric magnitudes should correspond to fluxes with at least a 10% accuracy, which is sufficient for the photometric correction required here. The photometric correction factors obtained were 0.76, 0.88, and 1.12 for the June 26, July 3, and July 17 spectra, respectively (see § 6). Since the uncertainties in the factors are of order 10% and since the *IUE* and optical spectra come from slightly different epochs, the corrections obtained from the factors are not clearly significant; nevertheless, the factors are adopted for correcting the optical spectra displayed in § 6 for whatever modest gains in accuracy may be achieved.

For the SN 1991T spectra, there was no need for photometric correction factors. Only one *IUE* spectrum was available, and it was combined with an optical spectrum from an epoch ~4 days earlier. The two spectra did not agree in the region of overlap, and so the *IUE* spectrum was simply scaled so that the net fluxes of the two spectra in this region would be equal (see § 7).

6. ANALYSIS OF THE SPECTRA OF SN 1990N

Figure 2 shows the stratified composition adopted for fitting the SN 1990N spectra. Below 14,900 km s^{-1}, the composition is a slightly modified version of the model W7 composition of Thielemann et al. (1986); only a selected group of velocity points from model W7 were used, and hence the piecewise linear appearance of the displayed abundance curves. Above 14,900 km s^{-1}, the W7 composition is homogeneous and consists of carbon, oxygen, and neon with mass fractions 0.475, 0.5, and 0.025, respectively. Experimentation showed that this composition was inadequate for fitting the SN 1990N observations, and therefore the rough nonrigorous fitting procedure outlined in § 3 was used to find a suitable homogeneous composition (hereafter the fitted outer composition) for the model from 14,900 km s^{-1} outward. (Fig. 2 cuts off at 15,500 km s^{-1}, but the fitted outer composition effectively extends to infinity.) The fitting procedure began with intermediate-mass elements in a mass ratio given by the total yield of these elements in the W7 composition (Thielemann et al. 1986, Table 5). The elements silicon through calcium had their mass abundance reduced by a factor of 10; the matter taken from these elements was changed into equal amounts of carbon and oxygen. The iron peak elements in the fitted outer composition also have

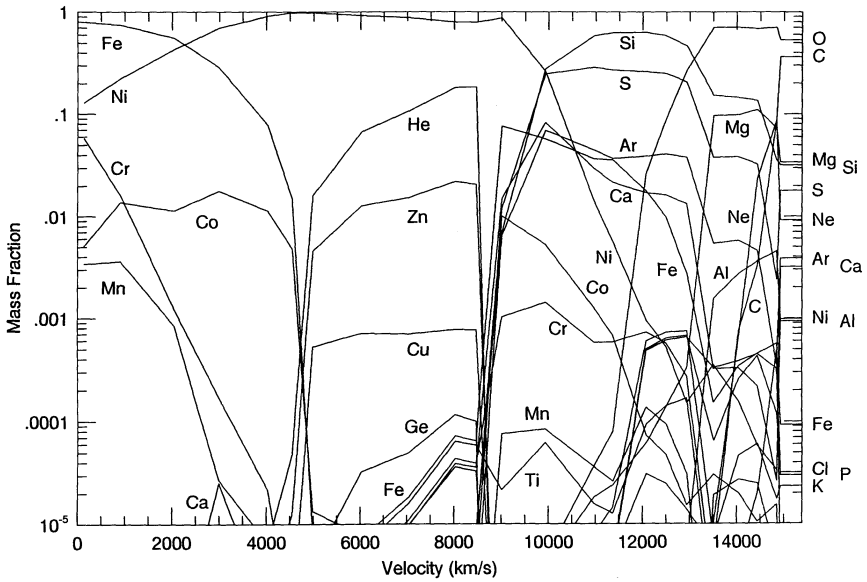

FIG. 2.—Composition used for the calculation of the synthetic spectra for SN 1990N. Below 14,900 km s^{-1}, the composition is essentially that of model W7 (Thielemann et al. 1986). Above 14,900 km s^{-1}, there is a homogeneous fitted outer composition that effectively extends to infinity. The composition is for the time of explosion. For any other epoch, the correct amounts of ^{56}Ni decay products must be calculated.

the mass ratio of the total yield of these elements in the W7 composition. The absolute amounts of the iron peak elements were varied for an overall fit to the three observed spectra being examined. The composition in Figure 2 is from the time of the explosion. About 95% of the total nickel abundance is radioactive ^{56}Ni; the percentage varies with velocity coordinate, but becomes constant at 95% in the fitted outer composition. The radioactive ^{56}Ni was converted into the proper amounts of parent and daughter elements for each spectrum epoch assuming that the nucleosynthesis took place 20 days prior to the *B* maximum on 1990 July 10.5 UT.

Figures 3*a*, 5, and 6 show the observed optical SN 1990N spectra for June 26 (14 days before maximum light), July 3 (7 days before maximum light), and July 17 (7 days after maximum light), respectively. Below about 3250 Å, there are *IUE* UV spectra from June 27, July 3, and July 14. The advantage of having complete spectra, from the near-UV region through to the near-IR region, outweighed concerns about fitting together spectra from slightly different epochs. The fact that the UV spectrum shows relatively slow change in shape during the period from June 26 to July 14 (Leibundgut et al. 1991a, Fig. 3) shows that the qualitative errors introduced by the fitting together of the spectra are probably small. The optical and UV spectra scales are in their observed ratio (see § 5), but the combined spectra have been scaled so that the highest observed flux is unity.

The synthetic spectra shown in Figures 3*a*, 5, and 6 were calculated as described in §§ 2 and 3. A synthetic spectrum is scaled to an observed spectrum by requiring that the integrated flux over the range 4000–7500 Å be the same for both spectra. The inner-boundary synthetic spectra are also shown in the figures (here and in § 7) in order to give some idea of the amount of flux reduction caused by absorption and backscattering in the model atmospheres. These inner-boundary synthetic spectra have mean slopes that are steeper by $\lesssim 30\%$ between 2500 and 10000 Å and by $\lesssim 10\%$ between 5000 and 10000 Å than the blackbody curves with the same temperatures as the inner boundary. It turned out with the adopted composition and temperature distribution that the synthetic Ca II H and K lines's absorption always extended too far to the blue. Therefore, an atmosphere cutoff velocity, $v_{\rm cutoff}$, was imposed on models to prevent this effect. The physical effect that prevents such an extended blue wing in the observed spectra may be a higher outer temperature, a NLTE effect, or in the case of the earliest spectrum a decrease in the density or calcium abundance profiles well below an exponential falloff. The cutoff velocity has no effect on any part of the spectrum besides the profiles of the Ca II H and K lines and sometimes the Ca II IR triplet. The parameters for the synthetic spectra displayed in the figures appear in Table 2.

6.1. *The June 26 Spectrum*

The synthetic spectrum fitted to the June 26 spectrum (Fig. 3*a*) is only of moderate quality. The model photosphere is located at 16,400 km s^{-1}, and so the synthetic line formation

TABLE 2

PARAMETERS FOR THE SN 1990N SYNTHETIC SPECTRA

PARAMETER	SPECTRUM IDENTIFICATION		
	June 26	July 3	July 17
v_1 (km s^{-1})	16000	11000	9000
T_1 (K)	11000	12000	11000
ρ_1 (g $cm^{-3} \times 10^{-13}$)	1.6	0.76	0.16
M_1 ($M_\odot$)	0.168	0.454	0.641
E_1 (ergs $\times 10^{51}$)	0.719	1.22	1.40
$v_{\rm ph}$ (km s^{-1})	16400	11200	6400
$T_{\rm ph}$ (K)	10600	11700	15400
$\rho_{\rm ph}$ (g $cm^{-3} \times 10^{-13}$)	1.4	0.70	0.36
v_2 (km s^{-1})	13500	9000	6200
T_2 (K)	14000	15000	16000
$v_{\rm cutoff}$ (km s^{-1})	40600	28800	24800

NOTE.—The parameters M_1 and E_1 are the mass and kinetic energy, respectively, of the ejecta above the point where the velocity is v_1. The parameters $v_{\rm ph}$, $T_{\rm ph}$, and $\rho_{\rm ph}$ are the velocity, temperature, and density, respectively, of the point in the atmosphere where $\tau_e = \frac{2}{3}$ (i.e., where the electron photosphere is located).

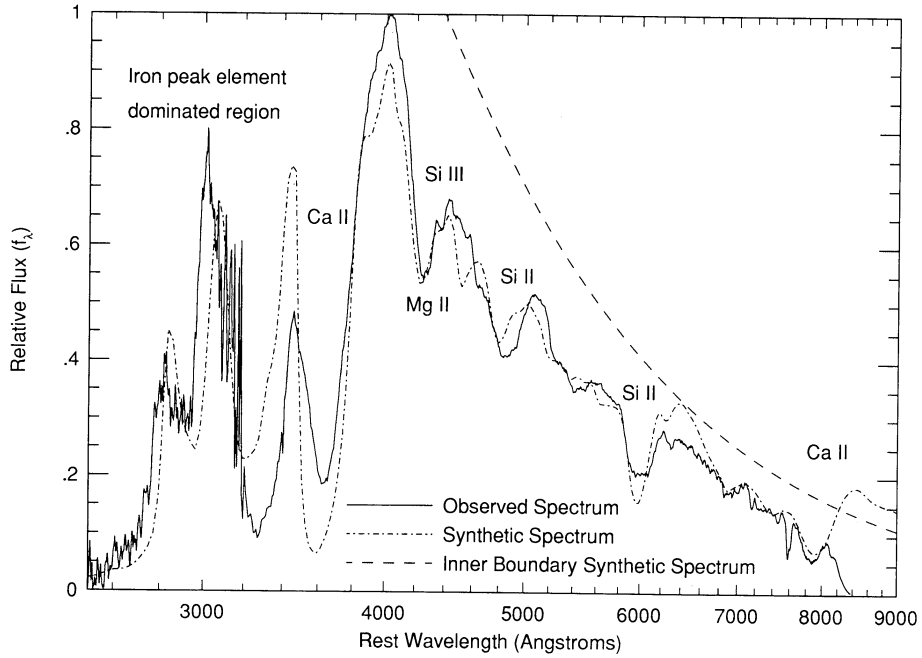

FIG. 3*a*

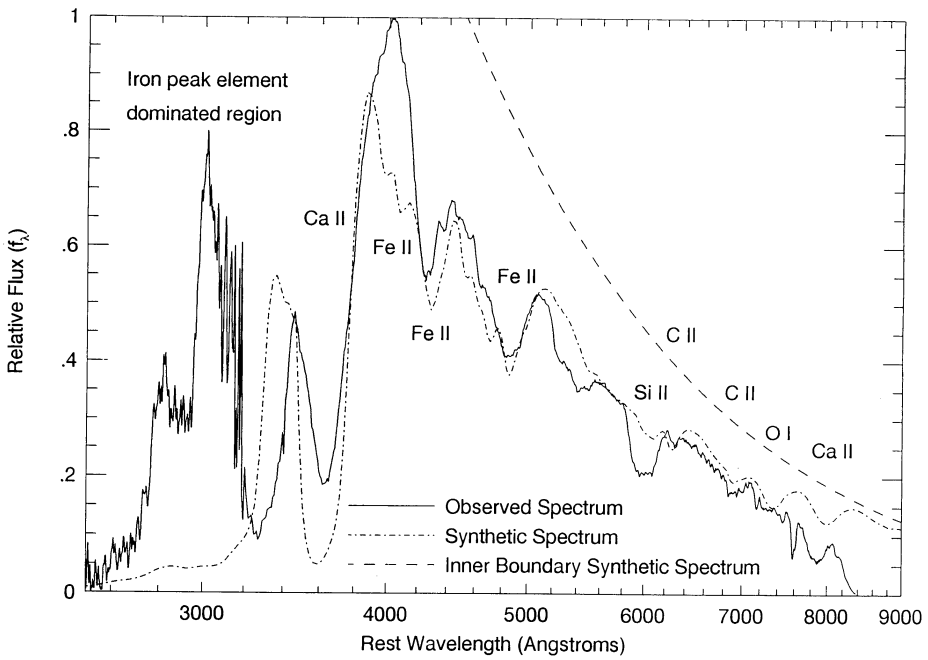

FIG. 3*b*

FIG. 3.—(*a*) June 26 observed and synthetic spectra for SN 1990N. Here and in the following spectrum figures (except for panel *b* of this figure), only the confidently identified observed absorptions are labeled. The sharp decline redward of ~8070 Å in the observed spectrum may be spurious according to the spectrum observer (Foltz 1992); thus, the disagreement from the calculated spectra in this region is not worrisome. (*b*) June 26 observed spectrum for SN 1990N and a synthetic spectrum calculated using a C-O–solar composition instead of the fitted outer composition in the ejecta above 14,900 km s^{-1}. Unlike all the other spectrum figures, the labels in this figure are intended only to designate the synthetic features, not as identifications in the observed spectrum.

mainly occurs in the fitted outer composition. The identifications of the Ca II H and K lines (with absorption centered at about 3600 Å) and the Ca II IR triplet (with absorption centered at about 7900 Å) are definite. If the blue edge of the observed H and K lines' P Cygni absorption is due only to the H and K lines, then a velocity of ~40,000 km s^{-1} is implied. (Note that all blueshift velocities quoted in this paper have been obtained using the relativistically correct Doppler shift formula.) The synthetic spectrum calculations show that weaker lines hidden beneath the H and K lines' absorption probably do not broaden this absorption; even the always obscured Si II λ3858 multiplet (which should be of comparable strength to the Si II λ6355 multiplet) does not have a significant broadening effect. Therefore, it is concluded that there probably is some ejecta at ~40,000 km s^{-1}. The Ca II IR triplet blue edge implies a slower velocity (~30,000 km s^{-1}), which is

expected, since the Ca II IR triplet is weaker (in LTE) than the H and K lines. There seem to be only two other supernova blue edges which give evidence for supernova ejecta velocities as high as $\sim 40{,}000$ km s^{-1}: the blue edge of the Ca II H and K lines' P Cygni absorption in a spectrum of the Type Ia supernova SN 1984A (Wegner & McMahan 1987; Branch 1987) from 7 days before maximum light (Leibundgut et al. 1991b) and the blue edge of what is almost certainly the Mg II resonance multiplet's P Cygni absorption in an *IUE* spectrum of the Type Ia supernova SN 1987A from day 1.658 after the explosion (Kirshner et al. 1987). In the synthetic spectrum, the cutoff velocity of 40,600 km s^{-1} prevents the H and K lines from destroying the flux peak at about 3450 Å. It should be noted that the W7 density distribution cannot produce a synthetic spectrum to fit the June 26 spectrum because this distribution cuts off at only 22,000 km s^{-1}. The cutoff of the W7 density distribution is an artifact of coarse zoning in the calculation of model W7, and so one cannot consider the cutoff as failure of the physical picture of model W7. The need to eliminate the W7 cutoff in the synthetic spectrum calculations was one of the main reasons for adopting an exponential density distribution.

The small absorption-like features in the June 26 spectrum at about 6300 and 6900 Å are possibly due to the C II $\lambda\lambda$6580 and 7243 multiplets, respectively. If the 6300 Å absorption-like feature is indeed due to carbon and the progenitor of the supernova was a C-O white dwarf, then unburned material is moving as slowly as $\sim 13{,}000$ km s^{-1}. This is about 2000 km s^{-1} slower than the carbon-rich fitted outer composition; the synthetic C II λ6580 multiplet absorption minimum corresponds to a velocity of $\sim 15{,}000$ km s^{-1}, i.e., the minimum velocity of the fitted outer composition. Unfortunately, the evidence for carbon is not strong; neither of the two absorption-like features is clearly fitted by the synthetic spectrum, and both features are nearly coincident with telluric absorptions which may obscure their appearances. Moreover, the synthetic spectrum also has an absorption at ~ 4500 Å due to the C II λ4743 multiplet, and there is no obvious corresponding absorption in the observed spectrum. Since the levels of C II λ4743 are closely connected to the levels of the other two C II multiplets, it seems unlikely that a C II λ4743 multiplet absorption could be suppressed by a NLTE effect; line blending perhaps could suppress such an absorption, but the synthetic spectrum does not show this effect. For these reasons, the identification of C II lines must be tentative.

The absorption at about 4250 Å is due to the Mg II λ4481 multiplet. The small absorption just redward of the Mg II absorption is identified as due to the Si III λ4560 multiplet by reason of continuity with the July 3 spectrum where the synthetic Si III absorption clearly fits the corresponding observed absorption. The absorptions at 4900 and 6000 Å are identified as due to the Si II $\lambda\lambda$5051 and 6355 multiplets, respectively. A strong Si II λ6355 multiplet is the characteristic feature of Type Ia supernovae. The 4900 Å absorption is not particularly well fitted; possibly lines of Fe II or Fe III should be stronger. Lines of S II may be at least partially responsible for the weak features in the 5000–5900 Å region, but the synthetic spectrum does not show this clearly. The region blueward of 3500 Å is dominated by many overlapping iron peak element lines that form a strong quasi-continuous expansion opacity. The synthetic flux in this region is strongly reduced below the inner boundary synthetic spectrum.

In analyzing the June 26 spectrum, synthetic spectra were also calculated using a C-O–solar composition (i.e., a solar composition with all H and He changed into equal amounts of C and O) instead of the fitted outer composition in the ejecta above 14,900 km s^{-1}. The best fit obtained is shown in Figure 3*b*. The parameters used for this synthetic spectrum are nearly the same as for the synthetic spectrum in Figure 3*a* (see Table 2), except that the temperature distribution was changed by using $T_1 = 10{,}000$ K, $T_{ph} = 9600$ K, and $T_2 = 13{,}000$ K. Thus, the atmosphere needed to be colder for the C-O–solar composition fit. The shape of the synthetic optical continuum seems in fact to be a little too cold for a good fit. Plausible fits are found for the observed 4300 and 4900 Å absorptions using Fe II lines, and the observed 6300 and 6900 Å absorptions are again fitted by C II lines. The synthetic Ca II IR triplet is now too weak, and there is a noticeable synthetic O I λ7773 absorption that does not correspond to anything in the observed spectrum. The synthetic Si II λ6355 absorption is a factor of about 10 too weak; over the range of reasonable temperatures used in the fitting procedure, the synthetic Si II λ6355 absorption was always a factor of about 10 too weak.

Overall, the fit to the optical with the C-O–solar composition is of only moderate quality. However, if LTE and the assumed temperature distribution were poor approximations, then one could argue that the C-O–solar composition was adequate to explain the optical spectrum. It is, in fact, likely that the observed 6000 Å absorption is affected by NLTE effects. The lack of any obvious emission feature shows that the line source function is somehow being suppressed, which cannot happen either with an LTE or a pure scattering source function. It is true that a P Cygni emission can be flattened and spread out and so become less conspicuous (with either an LTE or a pure scattering source function) if the line opacity is confined to a shell located well above the photosphere (e.g., Jeffery & Branch 1990, Fig. 6); however, opacity confinement in a "detached" shell is ruled out by the fact that the red edge of the flat bottom of the absorption corresponds to a velocity of $\sim 13{,}000$ km s^{-1}, which is slower than the fitted photospheric velocity of 16,400 km s^{-1}. Thus, a NLTE suppression of the line source function is probable. The flat bottom of the absorption may also be due to NLTE effects, but other explanations are possible. Given that NLTE effects are affecting the line, it is not unreasonable to suppose that solar silicon abundance with just NLTE enhancement can account for the strength of the absorption. For this reason, it cannot be categorically stated that the optical part of the observed spectrum demands newly synthesized silicon. However, if it is newly synthesized silicon that causes the absorption, then the blue edge of the absorption shows that newly synthesized elements are moving as fast as $\sim 25{,}000$ km s^{-1}.

The observed UV region presents a strong case for newly synthesized elements in the outer ejecta. Figure 3*b* shows no fit to the broad flux peak centered on about 3000 Å. This flux peak apparently cannot be fitted by iron peak elements in a solar ratio; the titanium, chromium, and iron lines suppress this feature relative to the flux peak centered on about 3450 Å for any temperature in the range ~ 5000–$10{,}000$ K. On the other hand, iron peak elements with Ni-Co at least a factor of 2, and more probably a factor of order 10 or more, more abundant than iron, do produce a 3000 Å flux peak (see Fig. 3*a*). Moreover, it is noteworthy that the particular ratio of iron peak elements chosen for fitted outer composition at least partially reproduces the shape of the observed 3000 Å flux peak. Since one would assume that iron peak elements in the supernova progenitor would have had something like the solar ratio of Ni-Co to iron of $\sim 1/20$ (Anders & Grevesse 1989), the

conclusion of a high ratio of Ni-Co to iron in the ejecta immediately implies that all or nearly all of Ni-Co results from ^{56}Ni production in the explosion and thus is newly synthesized.

The statements made above concerning the UV spectrum features resulting from the various iron peak elements were checked by calculating a number of synthetic spectra for isothermal expanding atmospheres each made of only one iron peak element. For temperatures between 5000 and 10,000 K, the expansion opacity produced by nickel, cobalt, and manganese allowed some sort of relative flux peak about 3000 Å, but iron, titanium, and chromium did not. A representative sample of these spectra showing only the iron, cobalt, and nickel spectra for 9500 K appears in Figure 4. The observed SN 1990N spectrum for July 3 appears in Figure 4 for general shape comparison.

The conclusion of the UV analysis is that at least some newly synthesized Ni-Co, and therefore other newly synthesized elements, must be present in the outer ejecta (i.e., above 15,000 km s^{-1} and probably out to at least 20,000 km s^{-1}), unless some strong NLTE effect is operative. This conclusion confirms the suggestion (based on a spectral analysis of an *IUE* spectrum of the Type Ia supernova SN 1981B) of Branch & Venkatakrishna (1986) that newly synthesized Ni-Co is present in Type Ia supernovae at velocities greater than ~12,000 km s^{-1}. Since incomplete burning to iron peak elements is likely to lead to abundant silicon production (see, e.g., the W7 part of the composition in Fig. 2), it seems likely that newly synthesized silicon is in fact mainly responsible for the strong Si II λ6355 absorption in the observed spectrum, and not NLTE effects. Because of the difficulty in making absolute abundance determinations in LTE with an assumed temperature distribution, it is not possible to say how much Ni-Co matter there is or how far outward it extends.

It must be remarked that the near-UV spectra of SN 1990N are somewhat different from the near-UV spectra obtained for other Type Ia supernovae (Blair & Panagia 1987, Fig. 1; Panagia & Gilmozzi 1991a, Fig. 1, and 1991b, Fig. 1; Kirshner et al. 1992; see § 7.2 below). There are some differences among the near-UV spectra of these other Type Ia supernovae, and the sample of near-UV spectra is small. Nevertheless, it is tentatively concluded that SN 1990N's near-UV spectra were atypical. A thorough study of available near-UV Type Ia spectra still needs to be done. At present, the similarities possessed by almost all near-UV Type Ia spectra (i.e., a strong decline in the blueward direction and a bumpy appearance) can be taken as weak evidence for the essential homogeneity of the near-UV Type Ia behavior. However, there is insufficient evidence to draw the conclusion that newly synthesized Ni-Co (and other elements) are present in the outer ejecta of all Type Ia supernovae.

6.2. *The July 3 Spectrum*

The synthetic spectrum fitted to the July spectrum (Fig. 5) is quite good. The identification of the Ca II H and K lines is again certain. The cutoff velocity prevents the absorption of the H and K lines from extending too far to the blue; the only other significant effect of the cutoff velocity is to narrow slightly the Ca II IR triplet's profile. The synthetic spectrum's consistency with the four absorptions identified as due to Si II (the Si II $\lambda\lambda$4130, 5051, 5972, and 6355 multiplets) and the two absorptions identified as due to Si III (the Si III $\lambda\lambda$4560 and 5740 multiplets) shows that these identifications are also certain. The structure in the region ~5200–5700 Å is due mainly to the S II $\lambda\lambda$5208, 5331, 5440, 5468, 5612, and 5654 multiplets. The absorption at 4300 Å is due mainly to the Mg II λ4481 multiplet. In addition to the lines identified in Figure 5, it seems

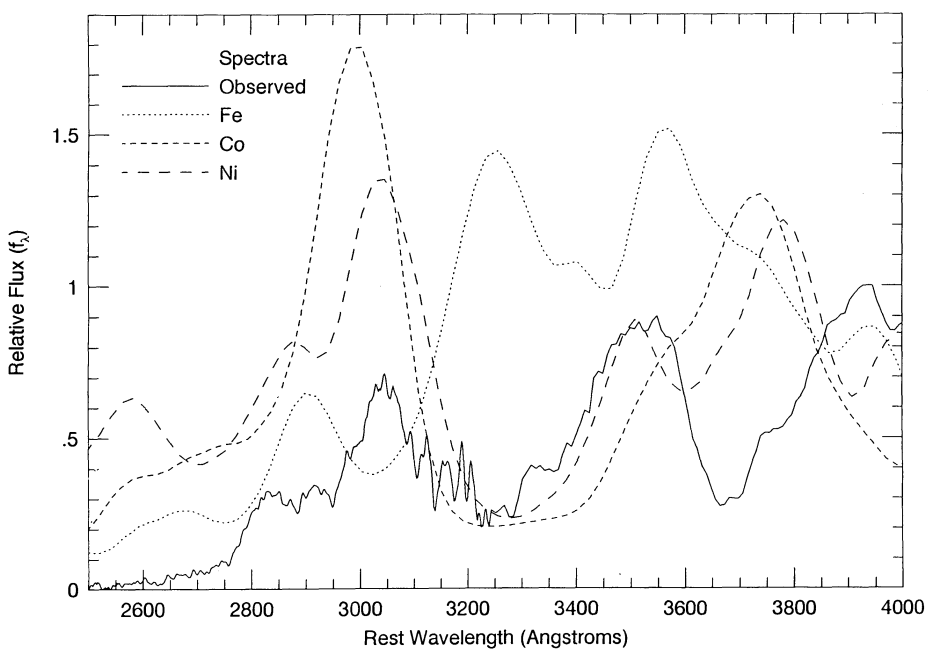

FIG. 4.—Synthetic spectra calculated for isothermal expanding atmospheres consisting of iron, cobalt, and nickel. Except for composition, temperature, and the replacement of LTE line source functions by pure scattering line source functions, the model parameters used for the calculations are the same as those used for the synthetic spectrum for July 3 (see § 6.2). The atmosphere temperature is 9500 K for all three cases. The July 3 observed spectrum is shown for general shape comparison. Each synthetic spectrum's overall scale was fixed by requiring that it have the same integrated flux over the (undisplayed) 4000–7500 Å range as the observed spectrum. The synthetic spectra were not intended to be fits to the observed spectrum.

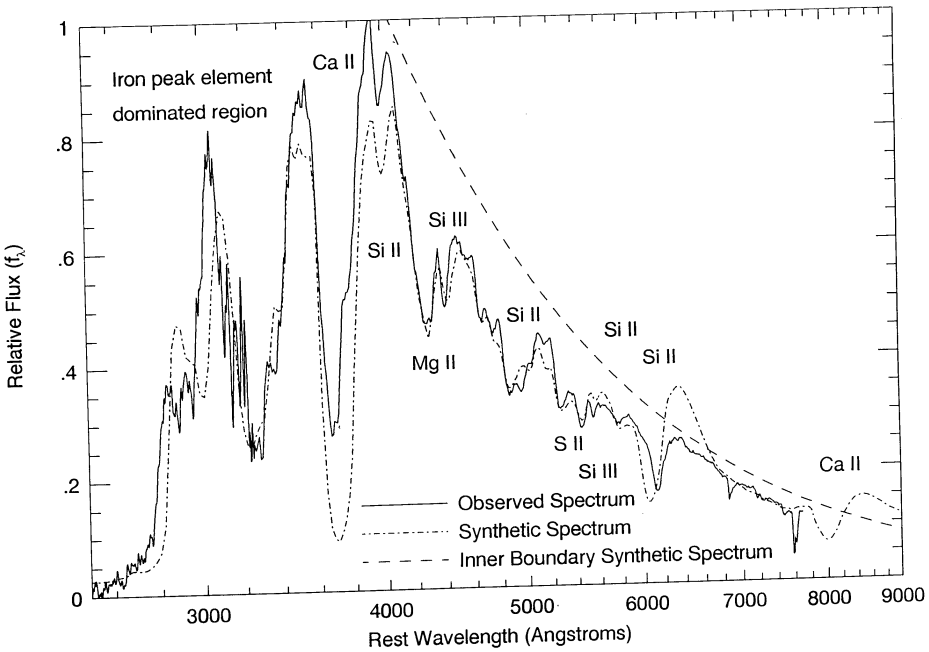

FIG. 5.—July 3 observed and synthetic spectra for SN 1990N

probable that the Fe III $\lambda\lambda$4404 and 5129 multiplets contribute to the 4300 and 4900 Å absorptions, respectively. (Note that here the mean multiplet wavelengths for iron peak elements are derived from Kurucz's line data files and may not quite agree with mean multiplet wavelengths from other sources.)

Overall, the July 3 spectrum is very similar to the June 26 spectrum, only with a lower photospheric velocity. From the synthetic fits it appears that the photospheric velocity has decreased by $\sim$5000 km s^{-1} between the two epochs (see Table 2). The smaller photospheric velocity causes less line blending, and so more small line features can appear. In the model atmosphere, the location of the photosphere is well into the real W7 composition region (see Fig. 2). If the model atmosphere were cut off at 15,000 km s^{-1}, the synthetic spectrum redward of 4000 Å would be qualitatively much the same; the Ca II IR triplet would vanish and the Si II λ6355 multiplet fit would improve. However, blueward of 4000 Å the synthetic spectrum would be radically different and would be a poor fit; the Ca II H and K lines' absorption would be much too slow, and the iron peak element dominated region would not look similar to the observations and would be insufficiently line blanketed. These facts confirm the analysis given in § 6.1 that requires Ni-Co–dominated iron peak elements moving at velocities of at least $\sim$15,000 km s^{-1}.

In the fitting procedure for the July 3 spectrum, the fitted outer composition was at first used for the entire atmosphere, and moderately good fits were obtained. However, changing to the real W7 composition below 14,900 km s^{-1} brought about a definite, although not an enormous, improvement. This suggests that the W7 composition in the velocity region about 11,000 km s^{-1} is close to correct.

6.3. *The July 17 Spectrum*

The July 17 spectrum (Fig. 6) is from 7 days after the maximum light. The discussion in § 4 shows that it is probable by this epoch that the photosphere has receded into the Ni-Co-Fe core of the ejecta if the core has a boundary velocity of $\sim$9000 km s^{-1}. Consequently, the blueshifts of the lines of intermediate-mass elements are limited by the lower bound on the velocity of these elements. The overall quality of the synthetic spectrum calculated with a composition that has no significant intermediate element abundance below 8500 km s^{-1} (see Fig. 2) is consistent with this picture. The synthetic Ca II IR triplet absorption is obviously much too fast compared with the observed line and would be faster still if there were no cutoff velocity. However, the blueshift of the synthetic absorption is here determined principally by the temperature distribution, not by abundance. The observed absorption minimum is blueshifted by $\sim$12,000 km s^{-1} from the mean line-center wavelength, and so is consistent with a core boundary velocity of $\sim$9000 km s^{-1}.

It is interesting to note that the Fe III $\lambda\lambda$4404 and 5129 multiplets now make the largest contributions to the synthetic absorptions that fit the observed 4300 and 5000 Å absorptions, respectively. The increase in the strength of the Fe III lines is, of course, due to the recession of the photosphere into the Ni-Co-Fe core, where in the time from July 3 to July 17 the iron fraction of the original ^{56}Ni abundance has increased from 5% to 15%.

The July 17 synthetic and observed spectra have several noteworthy discrepancies in addition to the poor Ca II IR triplet fit. Most of these discrepancies may be simply due to NLTE effects. As one can see from Table 2, the density of the model for July 17 at 9000 km s^{-1} was a factor of 9 lower than the photospheric density of the model for June 26. Lower density means lower electron density, and thus fewer thermalizing collisions. Therefore, the assumption of LTE should become poorer in the postmaximum epoch at least for those lines that are forced to form above $\sim$9000 km s^{-1}. Additionally, whatever accuracy the gray atmosphere temperature profile had at earlier times must diminish as more of the radioactive material appears above the photosphere. Recall that the gray atmosphere temperature was derived assuming radiative equilibrium and a central source of energy; with more radioactive energy deposition above the photosphere, radiative equilibrium becomes a poorer assumption.

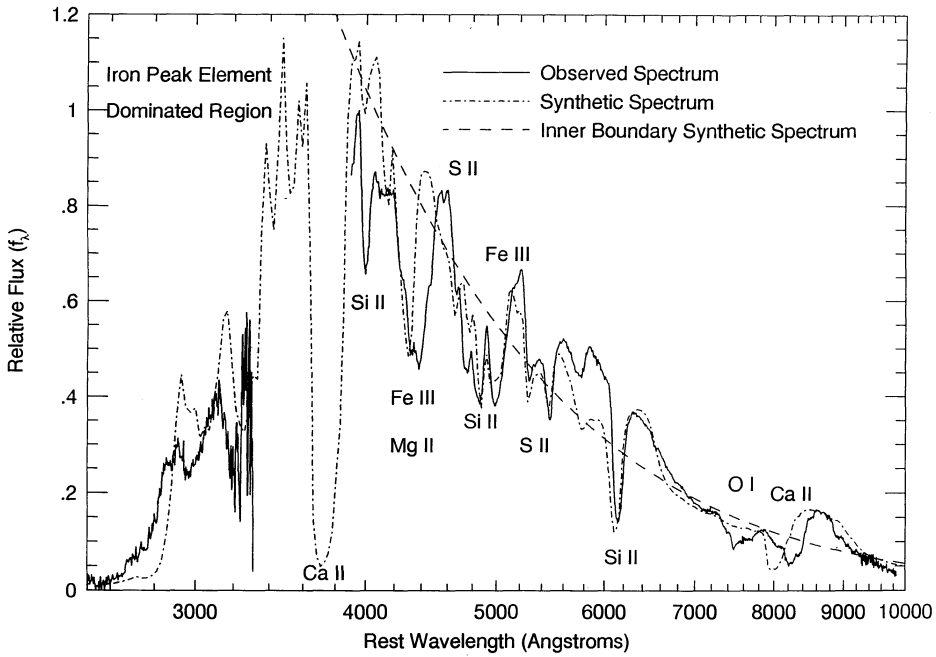

FIG. 6.—July 17 observed and synthetic spectra for SN 1990N

Besides the general invocation of NLTE effects, speculations can be offered concerning the causes of some of the more prominent discrepancies. Two such discrepancies between the synthetic and observed spectra are the flux excess of the synthetic spectrum in the region around 4000 Å and the lack of fit to the red side of the broad observed absorption centered at about 4300 Å. (The blue side of the 4300 Å absorption is mainly fitted, as noted above, by the synthetic absorption due to the Fe III λ4404 multiplet; there is also a small contribution from the Mg II λ4481 multiplet.) It is possible that both discrepancies are due to the weakness of Fe II lines in the synthetic spectrum. In § 7.3, stronger Fe II lines do give better fits to a postmaximum SN 1991T in the 4000–4600 Å region. The reason for these better fits is a higher iron abundance. It is possible that the iron abundance in the model composition for SN 1990N is too low in the velocity range $\sim$10,000–14,000 km s^{-1}. This suggestion, however, must be viewed cautiously, since the high iron abundance for SN 1991T is invoked to fit spectral behavior not seen in SN 1990N. If the Fe II lines are stronger than calculated, it may be that the identifications of the Fe III $\lambda\lambda$4404 and 5129 multiplets in the observed spectrum are not correct. A stronger Mg II λ4481 multiplet would also lessen the need for the Fe III λ4404 multiplet.

Another interesting discrepancy is the lack of a synthetic feature corresponding to the broad observed absorption centered near 7500 Å. This absorption seems to be typical of Type Ia supernovae from about maximum light to perhaps 15 days after maximum light (Branch et al. 1983, Figs. 1 and 8; Filippenko et al. 1992, Fig. 5; Phillips et al. 1992, Fig. 3; § 7.3 below, Fig. 10). Here the absorption seems to lack an emission feature, but it may be that the synthetic spectrum does not correctly locate the continuum level; whether an emission feature appears in other Type Ia supernovae is also not always clear. The absorption has usually been identified as due to the O I λ7773 multiplet with possible contributions from the Mg II λ7890 and Si II λ7850 multiplets (Branch et al. 1983, 1985; Harkness 1986; Wheeler et al. 1986; Harkness 1991a, b). None of these lines makes a significant contribution in the present LTE calculation. In the observed spectrum, it is very likely that there is in fact no significant contribution from the Mg II λ7890 multiplet. The lower level of the Mg II λ7890 multiplet is the upper level of the Mg II λ9226 multiplet, which does not give rise to an obvious feature in the July 17 spectrum or in the postmaximum spectrum of SN 1991T (see § 7.3). If the Mg II λ7890 multiplet were significant even in a very NLTE ion, it is hard to see how the Mg II λ9226 multiplet could fail to be significant. Since the Si II $\lambda\lambda$6355 and 5051 multiplets in the observed spectra have strengths that are roughly in the LTE ratio, it seems likely that the Si II λ7850 multiplet (which has levels closely related to the levels of the other two multiplets) would also have a strength in the LTE ratio. Given that the Si II λ7850 multiplet in LTE is only about 3% as strong as the Si II λ6355 multiplet, it follows that the Si II λ7850 multiplet probably does not contribute significantly to the 7500 Å absorption either. Thus, the 7500 Å absorption is probably almost entirely due to the O I λ7773 multiplet enhanced in strength by a NLTE effect or higher oxygen abundance than assumed in the model. It should be noted that Harkness (1991a, b) in self-consistent LTE calculations with model W7 is able to reproduce the O I λ7773 multiplet line in the maximum light spectrum of the Type Ia supernova SN 1981B; it is not obvious that he could do the same for a Type Ia supernova spectrum from 7 days after maximum light. The blue edge of the 7500 Å absorption is at $\sim$7300 Å, which shows that oxygen is probably moving as fast as 18,000 km s^{-1}. This result is consistent with the oxygen abundance of both the adopted SN 1990N composition and the actual W7 composition.

At epochs as early as $\sim$20 days after maximum light, Type Ia supernova spectra begin to make a transition from being dominated by P Cygni lines to being dominated by emission lines (e.g., Branch et al. 1983, Fig. 1; Filippenko et al. 1992, Fig. 6; Phillips et al. 1992, Fig. 3). Typical features in the early

emission spectra are a depression at about 5700 Å and an emission line at about 5900 Å; both these features are quite evident in the July 31 spectrum of SN 1990N (Filippenko et al. 1992, Fig. 6). An emission line at ~250 days after explosion near 5900 Å has been identified as due to [Co III] lines (Axelrod 1980a, b, 1988). Possibly these [Co III] lines are already the cause of the emission line in the spectra from ~20 days after maximum. In any case, the 5700 Å depression and 5900 Å emission line evident in the spectra from ~20 days after maximum may already be present in the July 17 observed spectrum of SN 1990N; if this is so, the emission line would then be the cause of the flux excess compared with the synthetic spectrum at about 5900 Å. The absorption in the synthetic spectrum at ~5750 Å is due to the Si II λ5972 multiplet and Fe III lines, however, because of the flux excess just discussed, this absorption may not correspond to any observed feature, or it may contribute to the possible 5700 Å depression. The 5700 Å depression has sometimes been tentatively identified as due to the Na I D lines. In LTE, however, these lines would be a factor of at least $\sim 10^3$ too weak. A large NLTE effect would be needed to make the Na I D lines sufficiently strong. Such an effect is possible, since the Na I abundance is typically nine or more orders of magnitude lower than the total sodium abundance in all the calculated atmospheres that have been considered for SN 1990N. The depression could, of course, be just an absence of flux emission between emission lines.

With the gray atmosphere temperature profile, the synthetic spectrum for the region blueward of 4000 Å is still strongly influenced by the ejecta moving faster than 15,000 km s^{-1} and thus is dependent on the fitted outer composition with its Ni-Co–dominated iron peak element ratio. The synthetic spectrum fit to the *IUE* UV spectrum is of only moderate quality.

7. ANALYSIS OF THE SPECTRA OF SN 1991T

The premaximum spectra of SN 1991T were remarkable in that they lacked the Si II λ6355 line that is the usual identifier of Type Ia supernovae. As discussed in § 6, this line was already present in the spectrum of SN 1990N 14 days before maximum light. Perhaps even more astonishing, the premaximum SN 1991T spectra lacked any obvious Ca II H and K spectral features; the Ca II H and K lines are strong resonance lines, and even with solar abundance they would give rise to strong spectral features with the gray atmosphere temperature laws used in this paper as Figure 3b demonstrates. The two strongest lines in the early spectra had absorptions at ~4200 and ~4900 Å. These lines have been identified in a NLTE analysis by Ruiz-Lapuente et al. (1992) (which, however, also used an assumed temperature law) as due to the Fe III λλ4404 and 5129 multiplets. Recall that Fe III lines were identified in the SN 1990N spectra, tentatively for July 3 and more confidently for July 17. Thus, the presence of Fe III lines in the SN 1991T spectra is probably not a unique phenomenon. Two possibilities arise for the cause of the discrepancy between the SN 1990N and SN 1991T spectra: somewhat different compositions or higher temperatures in the premaximum epoch in the SN 1991T ejecta. In fitting the SN 1991T spectra both a different composition and higher temperatures in the premaximum epoch turned out to be beneficial. The SN 1991T composition that was arrived at by the rough nonrigorous fitting procedure (see § 3) appears in Figure 7. This composition is constructed as follows. First, below 8500 km s^{-1}, the W7 composition is implemented. Above 8500 km s^{-1}, the W7 composition (out to 14,900 km s^{-1}) is somewhat simplified and is stretched outward to ~21,000 km s^{-1}. The abundances of nickel, iron, and some of the other elements in the ~8500–21,000 km s^{-1} region are adjusted. Above 21,000 km s^{-1} and effectively extending to infinity, the fitted outer composition used for SN 1990N is implemented. The abundances of the iron peak elements above 21,000 km s^{-1} are doubled. Finally, to account for the weakness of the intermediate-mass element lines, the abundances of silicon, sulfur, and argon are reduced everywhere by appropriate amounts. After these transformations, it turns out that calcium is a factor of order 10 less abundant and

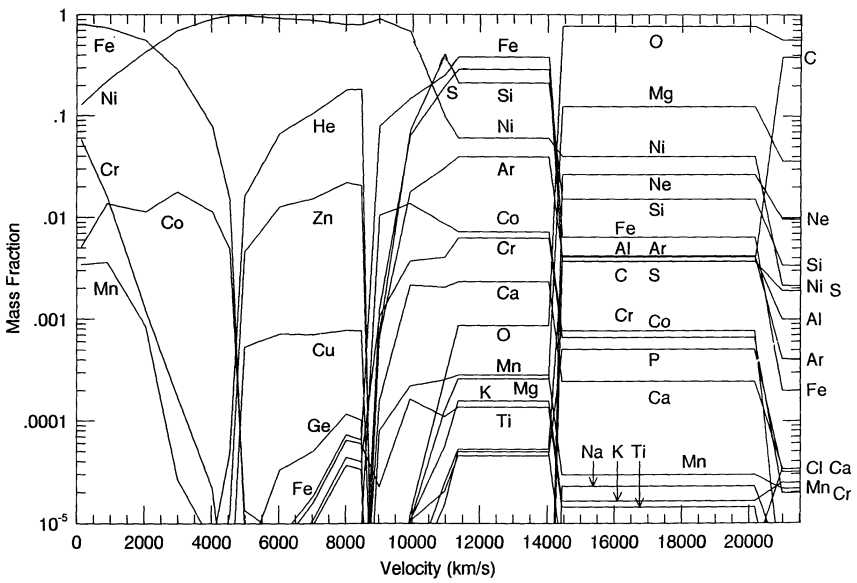

FIG. 7.—Composition used for the calculation of the synthetic spectra for SN 1991T. Below 8500 km s^{-1}, the composition is nearly that of model W7 (Thielemann et al. 1986). Between 8500 and 21,000 km s^{-1}, the composition is a heavily modified version of the W7 composition chosen to give fits to the observed spectra. Above 21,000 km s^{-1}, and extending to infinity effectively, is a modified version of the fitted outer composition used for SN 1990N. The composition is for the time of explosion. For any other epoch, the correct amounts of ^{56}Ni decay products must be calculated.

silicon is a factor of order 3 less abundant out to ~20,000 km s^{-1} than in the SN 1990N composition. The sulfur abundance in the range ~15,000–20,000 km s^{-1} turns out to be a factor of order 3 less abundant than in the SN 1990N composition. The radioactive ^{56}Ni was converted into the proper amounts of parent and daughter elements for each spectrum epoch, assuming that the nucleosynthesis took place 20 days prior to the *B* maximum on 1991 April 28.5 UT. It should be noted that the model composition was chosen to give reasonably good fits to all the observed spectra that are being analyzed; it is not necessarily the best composition for fitting any one of these spectra.

Figures 8, 9, and 10 display the observed and synthetic SN 1991T spectra for April 18–19, April 25 (April 29 for the UV region), and May 8–9, respectively. The *IUE* UV spectrum for April 29 was ~25% lower overall than the optical spectrum for April 25 in the region where the two spectra overlapped (~3060–3200 Å). This is not surprising, since the *U*-magnitude of Type Ia supernovae typically begins to decrease ~3 days before the *B* maximum epoch (Leibundgut 1988), which for SN 1991T was on April 28. Since the shape of the April 29 *IUE* UV spectrum was in good agreement with the shape of the April 25 optical spectrum in the region of overlap, it was decided to scale the UV spectrum so that the net fluxes of the UV and optical spectra agree. This seems a reasonable way to approximate the April 25 UV spectrum in view of the previously mentioned slow evolution of the shape of the SN 1990N UV spectrum (see § 6). As in § 6, all spectra have been scaled so that the highest observed flux is unity.

The SN 1991T synthetic spectra were calculated as described in §§ 2 and 3. A synthetic spectrum was scaled to an observed spectrum by requiring that the integrated flux over the range ~4500–7500 Å be the same for both spectra. Again the inner-boundary synthetic spectra are shown in the figures. Only for the May 8–9 synthetic spectrum (see § 7.3) as a cutoff velocity needed to prevent the Ca II H and K lines from extending too far to the blue; for the other two synthetic spectra, the cutoff velocities were chosen sufficiently large that they did not affect these spectra in any way. The parameters for the synthetic spectra are given in Table 3.

TABLE 3

PARAMETERS FOR THE SN 1991T SYNTHETIC SPECTRA

PARAMETER	SPECTRUM IDENTIFICATION		
	April 18–19	April 25	May 8–9
v_1 (km s^{-1})	13000	11000	9000
T_1 (K)	13200	12750	10750
ρ_1 (g cm^{-3} × 10^{-13})	0.89	0.34	0.12
M_1 ($M_\odot$)	0.311	0.454	0.641
E_1 (ergs × 10^{51})	1.01	1.22	1.40
v_{ph} (km s^{-1})	12700	9100	5600
T_{ph} (K)	13700	15800	17100
ρ_{ph} (g cm^{-3} × 10^{-13})	1.0	0.62	0.35
v_2 (km s^{-1})	11200	9000	4700
T_2 (K)	1600	1600	20000
v_{cutoff} (km s^{-1})	41100	33400	23300

NOTE.—See note to Table 2 for a description of some of the parameters.

7.1. *The April 18–19 Spectrum*

The April 18–19 spectrum in Figure 8 consists of two overlapping observations: there is a 3200–5800 Å spectrum from April 18 and a 4850–10100 Å spectrum from April 19 (see Table 1). In order to join the spectra smoothly, the two spectra were forced to have the same integrated flux in the region where they overlap. It is unfortunate that *IUE* UV spectra from the April 18–19 epoch could not be obtained, owing to spacecraft operational constraints. There exists an earlier optical spectrum for April 16 (Phillips et al. 1992, Fig. 3), but it covers only the region from 4600 to 7100 Å and is very similar in shape to the April 18–19 spectrum. Judging from the line profiles, the line formation region slowed by somewhere

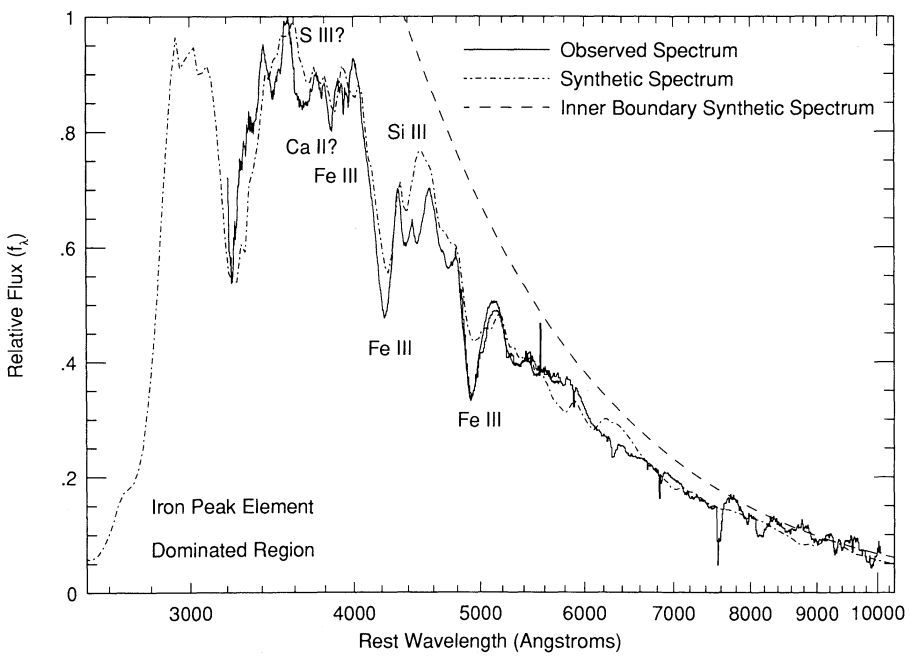

FIG. 8.—April 18–19 observed and synthetic spectra for SN 1991T. The sharp rise going in the blueward direction from ~3230 Å in the observed spectrum is very uncertain and may be spurious.

between 1000 and 2500 km s^{-1} in the time between April 16 and April 18.

The synthetic spectrum shown in Figure 8 is a reasonable fit to the observations. Clearly, the synthetic absorptions at about 4250 and 4950 Å due mainly to the Fe III $\lambda\lambda$4404 and 5129 multiplets, respectively, are too weak. Perhaps, as also suggested by the slow spectral evolution noted above, the region of high iron abundance in the supernova does not end as abruptly at ~14,000 km s^{-1} as in the adopted composition. In addition to Fe III lines, there is a contribution to the 4250 Å synthetic absorption from the Mg II λ4481 multiplet that is almost equal to the Fe III contribution. In the observed spectrum, the Mg II λ4481 multiplet may be less important, since no absorption due to the Mg II λ9226 multiplet (which should be about one-third as strong as the Mg II λ4481 multiplet in LTE) is observed. The small synthetic absorption at ~3850 Å is also due to Fe III lines. Given the Fe III line fits obtained here and the even better fits obtained for the April 25 spectrum (see § 7.2), it is concluded that Fe III lines are probably present in the observed spectra. This conclusion confirms the NLTE analysis of Ruiz-Lapuente et al. (1992) cited above.

The synthetic absorption at ~5800 Å is also due to Fe III lines. The absence of a corresponding observed absorption must be considered evidence against the presence of any Fe III lines in the observed spectrum. However, the suppression of an Fe III absorption near 5800 Å in the observed spectrum could simply be a NLTE effect; the NLTE synthetic spectra of Ruiz-Lapuente et al. (1992) are too noisy to decide this point clearly. It may be that the Fe III absorption is being suppressed by an early appearance of the 5900 Å emission line discussed in § 6.3; such a weak emission line may explain the odd shoulder-like appearance of the observed spectrum at about 5900 Å in both the April 18–19 and the April 25 spectra (see Figs. 8 and 9).

The ~5200–5700 Å region of the observed spectrum does not show any features that are clearly P Cygni absorptions or emissions. This region is mainly shaped by Si III, S II, and Fe III lines in the synthetic spectrum; it is possible that these lines are responsible for the shape of the observed ~5200–5700 Å region.

Blueward of about 3600 Å the synthetic spectrum is formed mainly by the iron peak element lines, with the line opacity in ejecta moving faster than 15,000 km s^{-1} being very significant. Note that in the model composition above 14,500 km s^{-1} the iron peak elements are again dominated by Ni-Co, not iron. The synthetic spectrum redward of about 3600 Å is formed mainly in the region from the electron photosphere at 12,700 km s^{-1} (see Table 3) to 15,000 km s^{-1}. In the inner part of this region, the largest contributor to the model composition is iron (see Fig. 7). Whether so much iron is needed to create Fe III features that match the observed features identified with Fe III cannot be definitively answered in an LTE analysis. One fact that does, however, argue for large iron abundance is that the Fe III LTE ionization fraction is in the range ~0.4–1 for all the atmosphere above the photosphere that is important for line formation; thus, not much more strengthening of the Fe III lines can be achieved by making more of the iron into Fe III.

The region around 3700 Å in the synthetic spectrum has significant contributions from the Ca II H and K lines and the S III $\lambda\lambda$3692, 3840, and 3950 multiplets. Because of the lack of clean line profiles in both the observed and the synthetic spectrum, however, only tentative identifications of Ca II and S III lines in the observed spectrum can be made.

There is a small synthetic absorption near 6100 Å due to the Si II λ6355 multiplet. No corresponding feature is evident in the observed spectrum. The suppression of the Si II multiplet in the observed spectrum may be due to NLTE effects or a somewhat different temperature or composition than that used to create the synthetic spectrum. There is a synthetic absorption at about 4400 Å due to the Si III λ4560 multiplet that makes a fair agreement with an observed absorption. If the observed absorption with minimum at 4390 Å is due to the Si III multiplet, then significant silicon abundance may exist in matter moving as fast as ~12,500 km s^{-1}; this conclusion is made taking line blending into account, since the blueshift corresponding to 170 Å is only 11,200 km s^{-1}. The observed absorption at about 4500 Å has not been identified; as will be seen in § 7.2 (see Fig. 9), this absorption weakens considerably by April 25.

There are a number of narrow features in the observed spectrum. The spike at ~5550 Å is a cosmic-ray event. The narrow absorption at ~5900 Å is due to the interstellar Na I D lines. Telluric lines account for the narrow absorptions at about 6200, 6800, and 7550 Å. The small features redward of ~7800 Å are probably instrumental noise. The smooth synthetic spectrum redward of 7800 Å is thus consistent with the observed spectrum.

7.2. *The April 25 Spectrum*

The synthetic spectrum in Figure 9 gives a good fit to the April 25 spectrum. Just as in the synthetic spectra of SN 1990N (see § 6), the synthetic region blueward of about 3600 Å is significantly shaped by the Ni-Co–dominated iron peak elements moving faster than 15,000 km s^{-1}; the goodness of the fit to the corresponding region of the observed spectrum (which includes the *IUE* UV spectrum from April 29) supports the idea that newly synthesized Ni-Co material dominates the iron peak element abundances in the outer ejecta. The SN 1991T *IUE* UV spectrum is slightly different from the maximum light *IUE* UV spectrum of SN 1990N (Leibundgut et al. 1991a, Fig. 3); the significance of this difference is not yet clear.

The Fe III $\lambda\lambda$4404 and 5129 multiplet identifications made in Figure 9 can be described just as for the April 18–19 spectrum (see § 7.1), except that the 4250 Å synthetic absorption is now almost entirely due to Fe III with only a small Mg II λ4481 multiplet contribution. As for the April 18–19 spectrum, there is a possibility of S III and the Ca II H and K absorptions contributing to the observed spectrum near 3700 Å.

The observed absorption at ~4400 Å is still present and is again identified as due to the Si III λ4560 multiplet. The observed and unidentified absorption at ~4500 Å has weakened considerably since April 18–19. At ~6150 Å there is now an observed absorption that can be identified as due to the similar Si II λ6355 multiplet.

The ~5200–5700 Å region of the observed spectrum again may be mainly shaped by Si III, S II, and Fe III lines.

7.3. *The May 8–9 Spectrum*

The observed May 8–9 spectrum in Figure 10 comes from 10–11 days after maximum light. From this time and thereafter the spectra of SN 1991T closely resemble the spectra of other Type Ia supernovae (Filippenko et al. 1992; Phillips et al. 1992); this similarity confirms the Type Ia classification of SN 1991T. The Si II λ6355 line and the S II lines in the 5000–6000 Å region, however, are notably weaker than in other Type Ia supernovae (Filippenko et al. 1992, Fig. 5). The appearance of

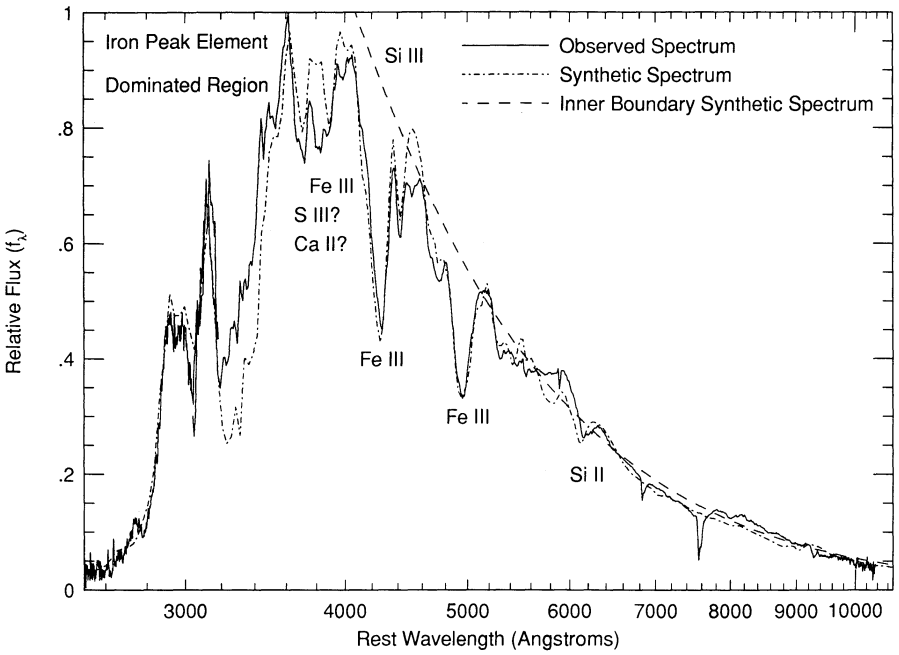

FIG. 9.—April 25 observed and synthetic spectra for SN 1991T

the Ca II H and K and the Ca II IR triplet absorptions is noteworthy because the blue edges of both features appear to be at blueshifts corresponding to $\sim$20,000 km s^{-1}. These blue edges provide evidence that calcium does extend far out into the ejecta. The lack of obvious calcium lines in the earlier spectra is probably attributable (as the analysis of these spectra suggested in §§ 7.1 and 7.2) to lower calcium abundance and to higher temperatures (which keep more calcium in the doubly ionized state) than in other Type Ia supernovae. If correctly identified, the Ca II blue edge velocity is the highest velocity observed for SN 1991T. Even in the earliest available spectra from April 16 (Ruiz-Lapuente et al. 1992, Fig. 2*a*), the blue edges of the lines attributed to the Fe III $\lambda\lambda$4404 and 5129 multiplets give velocities of only $\sim$20,000 km s^{-1} with uncertainties of $\sim$5000 km s^{-1}. The lack of evidence for material moving faster than $\sim$20,000 km s^{-1} does not imply that there was no such material. For SN 1990N it is the strong absorption due to the Ca II H and K lines in the spectrum from 14 days before maximum light that shows the existence of very fast material; SN 1991T does not have as early a spectrum and does not have lines as strong as the Ca II H and K lines of SN 1990N in the earliest spectra available.

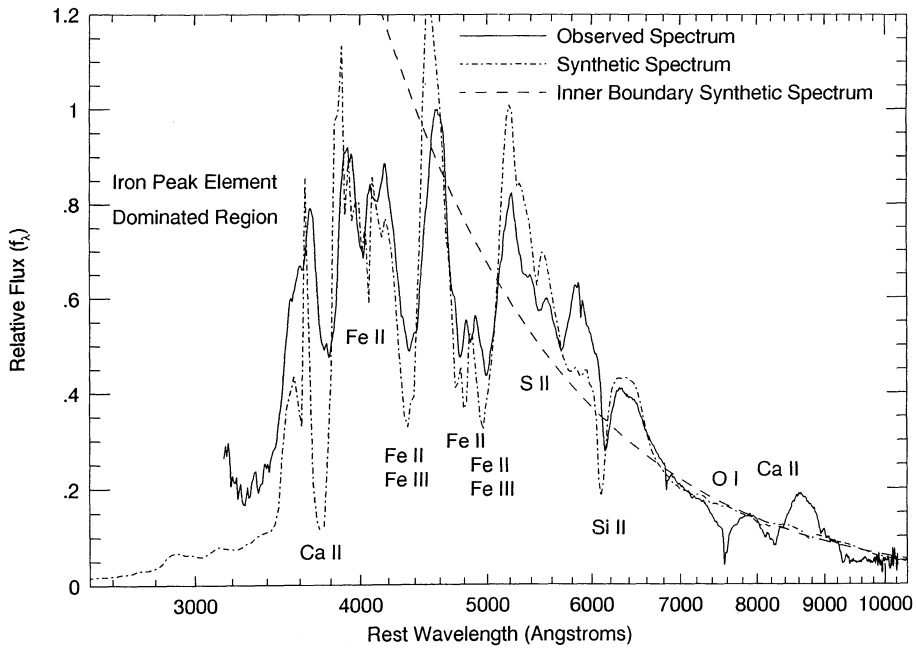

FIG. 10.—May 8–9 observed and synthetic spectra for SN 1991T

The synthetic spectrum in Figure 10 is only a moderately good fit to the observations. As in the case of the fit to the July 17 spectrum of SN 1990N, the chief cause of the discrepancies is probably the increasing NLTE nature of the supernova atmosphere as the density of the main line formation region falls with time. In May 8–9 synthetic spectrum, Fe II lines play a significant role, which they did not do (but perhaps should have) in the July 17 synthetic spectrum of SN 1990N (see Fig. 6). The reason for the stronger Fe II lines is partially the slightly lower temperature above the Ni-Co-Fe core used to create the SN 1991T spectrum (see T_1 in Tables 1 and 2) but is mainly the much greater iron abundance in the composition used to create the SN 1991T synthetic spectra (compare Figs. 2 and 7). As with the July 17 SN 1990N case, the synthetic spectrum does not fit the emission feature centered at ~ 5900 Å. Again an emission line (possibly due to [Co III]) may be responsible for the discrepancy. The synthetic Ca II H and K lines and Ca II IR triplet are too strong and too weak, respectively, to fit the corresponding observed features; a NLTE effect must be invoked to explain this discrepancy. The observed absorption (i.e., the broad absorption, not the superposed narrow telluric line) identified with the O I λ7773 multiplet is not at all fitted by the synthetic spectrum; a NLTE effect or higher oxygen abundance must be invoked to account for this. The blue edge of the O I absorption shows that probably there is oxygen moving at a velocity of $\sim 18{,}000$ km s^{-1} just as in SN 1990N.

Redward of ~ 4500 Å, the synthetic spectrum is formed mainly by the matter moving slower than 15,000 km s^{-1}. Blueward of ~ 4500 Å, the outer ejecta has a greater role in the formation of the synthetic spectrum. The synthetic spectrum shows that the observed spectrum is consistent with the model W7 prediction of a Ni-Co-Fe core with boundary velocity ~ 9000 km s^{-1}.

Many of the synthetic absorptions seem a little too blueshifted compared with the observed absorptions. In the case of the small synthetic absorption near 5450 Å due to S II lines, the excess blueshift may be due to a failure of LTE line blending. A general decrease in the blueshifts can be achieved by lowering the temperature, but this also increases strengths of the synthetic Ca II, Fe II, and Si II lines, and these lines are already too strong. Numerical experiments showed that increasing the abundances of iron and the intermediate-mass elements in the velocity region near 10,000 km s^{-1} was not a panacea, although such an increase could not be ruled out. The failure to cure the blueshift problem is probably due either to an incorrect temperature distribution with radius or to the lack of NLTE effects in the calculations.

8. ABSOLUTE *B* MAXIMUM AND DISTANCE DETERMINATIONS USING THE EXPANDING PHOTOSPHERE METHOD

In this section the expanding photosphere method (EPM) has been applied to SN 1990N and SN 1991T. The EPM is a procedure for using synthetic spectra for absolute flux and distance determinations. This method has been applied in the past to Type Ia supernovae using synthetic spectra calculated for somewhat simpler models than those used here (e.g., Branch & Patchett 1973; Kirshner et al. 1976; Branch 1977, 1979; Branch et al. 1983). For Type II supernovae, more advanced NLTE EPM determinations have been made recently by, e.g., Chilukuri & Wagoner (1988), Höflich (1988), Eastman & Kirshner (1989), Schmutz et al. (1990), and Schmidt, Kirshner, & Eastman (1992). In its most direct form, the EPM luminosity L for a supernova is calculated from a synthetic spectrum, and the EPM distance is obtained from the equation

$$d = \left(\frac{L}{4\pi f}\right)^{1/2}, \tag{20}$$

where f is the extinction-corrected total flux observed at Earth. The EPM's name comes from the fact that the radius of a supernova's photosphere can be found from the photospheric velocity (determined by a spectral analysis that is independent of the supernova's absolute luminosity) and the time from explosion. Knowing the photosphere's radius then allows an absolute synthetic flux to be calculated for the supernova from a model. Because of the lack of a self-consistent LTE treatment of the radiative transfer, the lack of the correct Type Ia supernova models, and the uncertainty in the explosion times of SN 1990N and SN 1991T, it is estimated that there is an uncertainty of a factor of order 2 in any synthetic flux calculated here. Consequently, the distance determination made here for SN 1990N and SN 1991T are also uncertain by factors of order 2.

Instead of using equation (20) (which requires knowledge of the flux at Earth at all wavelengths), the distance determinations have been made using the magnitude formula

$$d = 10^{0.2(B - M_B) - 5} \text{ Mpc}, \tag{21}$$

where B is an apparent B magnitude (corrected for foreground Galactic extinction) and M_B is a synthetic absolute B magnitude. The apparent B magnitudes were calculated for the epochs of the spectra of SN 1990N and SN 1991T from the Type Ia supernova template B light curve fitted to the observed B light curves of the supernovae. The synthetic absolute B magnitudes were calculated from the six synthetic spectra displayed in §§ 6 and 7 with the same procedure (discussed in § 5) used to obtain spectrum-derived magnitudes from observed spectra. The absolute B maxima for the supernovae were calculated by using the synthetic spectrum B magnitudes to fix the absolute scale of the template B light curve.

The calculated absolute B maxima and the EPM distances appear in Table 4. The fact that the determinations for each supernova vary with the spectrum used to obtain them shows clearly the uncertainty of the EPM as applied here. Better final determinations can be made by taking the means of the premaximum spectrum determinations. The determinations from the postmaximum spectra have been neglected, since, as discussed in §§ 6.3 and 7.3, the LTE condition used in the calculations is expected to become poorer in the postmaximum epoch; the fact that the premaximum values are more consistent with one another than with the postmaximum values supports this expectation. The mean distance determinations are consistent with the literature values cited in Table 4 within factors of 2. The mean absolute B maximum determinations are consistent with the notion that Type Ia supernovae are standard candles and their average, -19.9 ± 1 mag, is a determination of the standard candle Type Ia supernova absolute B maximum. If the expression for the absolute B maximum derived from Miller & Branch (1992) (see Table 4) is inverted for H_0 using -19.9 mag, a value of 50 km s^{-1} Mpc^{-1} with an uncertainty of a factor of order 2 is obtained. This value is consistent with Hubble constant values in the literature: ~ 25–100 km s^{-1} Mpc^{-1}.

Because of the large uncertainties, the EPM determinations

TABLE 4

DISTANCE AND ABSOLUTE *B* MAXIMUM DETERMINATIONS

Designation	Distance (Mpc)	Absolute *B* Maximum (mag)
SN 1990N		
June 26	34	-20.0 ± 1
July 3	27	-19.5
July 17	47	-20.7
Means for June 26 and July 3	30	-19.8
SN 1991T		
April 18–19	20	-19.9 ± 1
April 25	23	-20.2
May 8–9	30	-20.7
Means for April 18–19 and April 25	22	-20.0
Literature Values		
NGC 4639 (SN 1990N)	20.6[a]	...
NGC 4527 (SN 1991T)	13.0[b]	...
Means	...	$-19.0 \pm 0.3 + 5 \log (H_0/75)$[c]

NOTE.—The uncertainty of a synthetic flux is assumed to be a factor of order 2. Consequently, the uncertainty in the distance determinations is also a factor of order 2, and the uncertainty in the absolute *B* maximum determinations is ~1 mag. The mean determinations have the same uncertainties as the individual spectrum determinations.

[a] Pierce & Tully 1988.

[b] Tully et al. 1992.

[c] Derived from Miller & Branch 1992.

made here are not of great interest as new determinations. Their primary importance is that their consistency with literature values supports the Type Ia supernova models and the radiative transfer technique that have been adopted in this paper.

In future work there is potential for improving the EPM for Type Ia supernovae. A detailed self-consistent NLTE treatment of the radiative transfer would elminate much of the physical uncertainty. If one then had a sufficiently good Type Ia supernova model, EPM determinations of the same accuracy as for Type II supernovae may be possible. Such an improved EPM for Type Ia supernovae would eliminate the need to assume that Type Ia's are standard candles in distance and Hubble constant determinations. Type Ia supernovae have the advantage over Type II's in such determinations by having absolute *B* maxima that are on average brighter by ~1.8 mag with no parent galaxy extinction corrections considered (Miller & Branch 1990); thus, Type Ia's can be used to greater distances. It should also be pointed out that Type Ia supernovae in the present era of systematic supernova searches are not uncommon observational events: 28 of the 60 supernovae discovered in 1991 were Type Ia's.

9. CONCLUSIONS AND DISCUSSIONS

The analyses of SN 1990N and SN 1991T give rise to a number of conclusions.

1. SN 1990N has matter moving as fast as ~40,000 km s^{-1}. SN 1991T has matter moving as fast as ~20,000 km s^{-1}. In both cases, matter at higher velocities is possible.

2. The exponential density profile with *e*-folding velocity 3160 km s^{-1} suggested by the deflagration and delayed/late-detonation explosion models was adequate for calculating fits to the observed spectra. It must be noted, however, that deficiencies in the adopted density profile can easily be obscured by the adjustment of other model parameters.

3. The ratios of the iron peak elements in the outer ejecta (i.e., ejecta moving faster than ~15,000 km s^{-1}) of the model compositions give good fits to the UV regions of the spectra of both SN 1990N and SN 1991T. The iron peak element abundances in both cases are dominated by Ni-Co. Therefore, it is probable that newly synthesized Ni-Co dominates the iron peak element abundances in the outer ejecta of the two supernovae. This result, along with the evidence for newly synthesized silicon moving as fast as 25,000 km s^{-1} in SN 1990N suggests that in both supernovae some nuclear burning continues into the outer ejecta or that newly synthesized elements are mixed into the outer ejecta. At present, it is not known whether newly synthesized elements need to be invoked in the outer ejecta of all Type Ia supernovae.

If mixing is responsible for the newly synthesized elements in the outer ejecta, it seems probable that the mixing would have to yield compositions that were fairly homogeneous or at least spherically symmetric. This conclusion is reached because of the first-order consistency between the synthetic spectra calculated in spherical symmetry and the observations. Although numerical experiments remain to be done, one would guess that gross aspherical inhomogeneities would lead to strange features that are not like those of ordinary P Cygni lines or line blends. An element abundance inhomogeneity may lead to a strange feature that was repeated in every line belonging to that element. An inhomogeneity in a radioactive element's abundance may lead to extra line emission features in the lines of many elements. For example, the satellite emission features

that accompanied some of the P Cygni emissions in the Type II supernova SN 1987A spectra have been attributed to an aspherical distribution of radioactive ^{56}Ni due to mixing or some other cause (Lucy 1988; Phillips & Heathcote 1989; Hanuschik & Thimm 1990; Hanuschik 1991).

4. The unmodified model W7 cannot be a completely correct model for all Type Ia supernovae because it has no matter moving faster than 22,000 km s^{-1} and no newly synthesized elements moving faster than 15,000 km s^{-1}. On the other hand, the W7 composition below 15,000 km s^{-1} seems to account quite well for the SN 1990N spectra although not for SN 1991T spectra. Delayed-detonation models for Type Ia supernovae (Khokhlov 1991a, b; Woosley 1991) or pure detonation models in white dwarfs of less than the Chandrasekhar mass (Shigeyama et al. 1992) are able to produce intermediate-mass elements at velocities greater than 25,000 km s^{-1}. However, it is not clear yet whether such models can also produce iron peak elements dominated by Ni-Co in ejecta moving faster than 15,000 km s^{-1}. The late-detonation models of Yamaoka et al. (1992) do produce iron peak elements dominated by Ni-Co in the ejecta moving faster than 15,000 km s^{-1}; preliminary synthetic spectrum calculations with these models are promising for fits to the SN 1990N spectra.

For both SN 1990N and SN 1991T, the postmaximum spectra examined here are consistent with the model W7 prediction of a Ni-Co-Fe core boundary velocity of $\sim$9000 km s^{-1}. With the exponential density distribution adopted in this paper, the core would have a mass of $\sim 0.76\ M_{\odot}$; the actual model W7 core mass is $0.78\ M_{\odot}$ (Thielemann et al. 1986, Fig. 2). In regard to the location of the core, the terminal line velocities (i.e., the final line velocities before disappearance of the P Cygni absorptions) of the Si II λ6355 line from SN 1990N, SN 1991T, and other Type Ia supernovae provide important evidence. From compilations of Si II λ6355 line evolution (Branch, Drucker, & Jeffery 1988; Leibundgut et al. 1991a; Benetti & Barbon 1991; Phillips et al. 1992), it appears that the terminal line velocities never get smaller than $\sim$8500 km s^{-1}; in 15 out of the 30 published cases, the last observed, but not necessarily terminal, line velocities are greater than $\sim$10,000 km s^{-1}. Since strong lines would have line velocities larger than the minimum allowed by composition and since the determination of the terminal line velocity is complicated by incomplete observational coverage and the transition of the supernova spectrum to an emission-line spectrum, it is at least possible that all the data are consistent with a Ni-Co-Fe core boundary velocity of $\sim$8500–9000 km s^{-1}. A careful synthetic spectrum analysis of all the Si II line observations may lead to stronger constraints on the core boundary velocity. Since the core boundary velocity is unquestionably an important parameter for the explosion calculations, such a project would be of great interest.

Given the partial success of model W7 in explaining the SN 1990N spectra, it seems very likely that some version of the deflagration or delayed/late-detonation models will be able to account for the results of the LTE analysis of SN 1990N. Since SN 1990N is apparently a typical Type Ia supernova, the model that accounts for the SN 1990N behavior will probably become a fiducial Type Ia supernova model. For those calculating explosion models, the challenge is to produce such a model in a physically plausible manner.

5. As shown by Filippenko et al. (1992) and Phillips et al. (1992), the postmaximum spectra of SN 1991T are qualitatively typical of Type Ia supernovae. Phillips et al. (1992) also shows that the light-curve behavior of SN 1991T through the first $\sim$100 days after explosion is only slightly different from that of other well-observed Type Ia supernovae. However, the premaximum spectra of SN 1991T are qualitatively different from the premaximum spectra of other Type Ia's including SN 1990N. These premaximum spectra from other supernovae are recognizably similar to each other. The analysis given here shows that the premaximum SN 1991T spectra, although clearly different from those of SN 1990N, are not so extremely different as it first appears. The overall shape of the optical and near-IR regions of the premaximum spectra of the two supernovae are quite similar (see Fig. 1). Lines due to silicon sulfur, and calcium that are easily identified in the premaximum spectra of SN 1990N may have had an effect in the SN 1991T spectrum from 10 days before maximum light. The analysis of SN 1990N showed the possibility of some Fe III lines in that supernova's premaximum and postmaximum spectra; thus, the Fe III lines identified in the premaximum and postmaximum spectra of SN 1991T, instead of being unusual (except maybe in strength), may rather have been typical of Type Ia supernova spectra. Given these results, the explosion history of SN 1991T is probably not fundamentally different from that of other well-observed Type Ia's. A variation of the model that will account for SN 1990N will probably also account for SN 1991T.

6. The two most prominent lines in the premaximum spectra of SN 1991T are identified as due to the Fe III $\lambda\lambda$4404 and 5129 multiplets. In creating synthetic spectrum fits to these lines, both higher temperatures in the premaximum epoch (compare the T_1 and T_{ph} values in Tables 2 and 3) and a larger iron abundance for SN 1991T relative to SN 1990N had to be invoked. Given the weakness of the silicon, sulfur, and calcium lines in SN 1991T realtive to SN 1990N and other Type Ia supernovae, a SN 1991T composition that has less silicon, sulfur, and calcium and more iron than typical Type Ia compositions seems probable. The fitted composition for SN 1991T reported in § 7 suggests that relative to the SN 1990N composition, silicon was underabundant overall by a factor of $\sim$3 and calcium was underabundant overall by a factor of $\sim$10 in the SN 1991T composition. The overall sulfur abundance was probably lower in SN 1991T by a factor of order 3, but the complications of stratification make this an even less certain estimate. Higher temperatures in the premaximum SN 1991T atmosphere may have been a consequence of compositional differences. It should be remarked that given the shape similarity of the premaximum optical and near-IR regions of the spectra of SN 1990N and SN 1991T (see § 5), the temperature difference between the two supernovae determined from the fitting procedure may be somewhat too large.

The composition that has been used to create the synthetic spectra for SN 1991T (see Fig. 7) seems to be adequate to explain the observations, but the question of its physical plausibility arises. In the W7 composition there is a velocity region around 12,000 km s^{-1} where iron abundance exceeds nickel abundance (see Fig. 2). Therefore, it may be possible in a nucleosynthetic calculation for iron to become the dominant element above the Ni-Co-Fe core in the velocity range $\sim$11,000–14,000 km s^{-1} just as in the adopted SN 1991T composition. The late-detonation models show that it is then possible for Ni-Co to become the dominant iron peak elements in the ejecta above $\sim$15,000 km s^{-1}. It must, however, be emphasized that the non–self-consistent LTE calculations done here are not sufficiently conclusive for the Figure 7 composition to be regarded as more than suggestive.

For their NLTE calculations for SN 1991T, Ruiz-Lapuente et al. (1992) used a model outer atmosphere consisting of only ^{56}Ni and daughter elements. Their model was suggested by older nucleosynthetic models (model C8 of Nomoto et al. 1984 and model 3 of Woosley & Weaver 1986b; the model 3 composition is shown in Fig. 4 of Harkness 1991a) which would now be called late-detonation models in which Ni-Co-Fe matter dominates the outer composition. Because the iron in the model of Ruiz-Lapuente et al. comes entirely from the ^{56}Ni decay chain, the iron abundances were everywhere only a few percent by mass in the premaximum epoch, whereas here it was assumed that the iron abundance mass fraction was 0.4 in the range $\sim$11,500–14,000 km s^{-1} and less than 0.01 above 14,500 km s^{-1} (see Fig. 7). The difference in iron abundances used to obtain fits to the Fe III lines is accounted for by Ruiz-Lapuente et al.'s use of higher temperatures and densities, and the greater outward extension of iron abundance mass fraction greater than 0.01 in their model. Besides Fe III lines, Ruiz-Lapuente et al. identify the small feature at about $\sim$5300 Å in the premaximum spectra as an absorption due to Ni III lines. If correct, this identification supports the idea of an iron peak element–dominated late detonation. The identification, however, is not certain; as suggested in §§ 7.1 and 7.2, Si III, S II, and Fe III lines may account for the spectrum behavior in the $\sim$5200–5700 Å region.

7. Although stratified compositions of intermediate-mass elements above the Ni-Co-Fe core were used in the models and were found adequate, it is not evident that a high degree of stratification is required in the supernova ejecta. In the case of SN 1990N, the homogeneous fitted outer composition was adequate to explain the earliest spectrum. This same spectrum showed some evidence for significant (presumably not newly synthesized) carbon moving at $\sim$13,000 km s^{-1}, which is slower than predicted by model W7. For the later SN 1990N observed spectra, synthetic spectra that were largely formed in the $\sim$9000–15,000 km s^{-1} region of the adopted SN 1990N composition gave good fits. It is not evident, however, that the stratification in this region was of major importance. For SN 1991T, the adopted composition had major discontinuities in abundances at $\sim$14,250 km s^{-1}. However, as suggested in § 7.1, these discontinuities may be much too abrupt. Clearly, a closer examination of observations for evidence for or against stratification above the Ni-Co-Fe core is merited; such evidence would have important implications for the modeling of the burning front propagation and/or for the existence of tuburlent mixing in the ejecta containing the intermediate-mass elements.

8. Using the EPM, determinations of the distances (30 and 22 Mpc with uncertainties of factors of order 2) and the absolute B maxima (-19.8 ± 1 mag and -20.0 ± 1 mag) have been made for SN 1990N and SN 1991T. The absolute B maximum determinations are consistent with the notion that Type Ia supernovae are standard candles, and their average, -19.9 ± 1 mag, is a determination of the standard candle Type Ia supernova absolute B maximum. This standard candle Type Ia absolute B maximum is consistent with a Hubble constant in the range $\sim$25–100 km s^{-1} Mpc^{-1}. The overall consistency of the EPM determinations with literature values supports the Type Ia supernova models and the radiative transfer technique that have been adopted in this paper. It is possible that the EPM applied to Type Ia supernovae can be made to yield much more accurate determinations than have been made here.

It should be noted that other methods for distance determinations using Type Ia supernovae that depend directly on the heating of the ejecta by the decays of ^{56}Ni and ^{56}Co (Arnett, Branch, & Wheeler 1985; Branch 1992; Leibundgut & Pinto 1992) may turn out to be superior to the EPM.

9. Since the nature of the Type Ia supernova burning front is most revealed in the ejecta layers where the burning was incomplete, premaximum spectra which are formed in these layers are of great value in understanding the explosion mechanism, and consequently the progenitors, of Type Ia supernovae. Thus, it is important to acquire the fullest possible spectral coverage in both time and wavelength of any Type Ia discovered well before maximum light. Equally complete photometric coverage is also obviously greatly desired for determining the luminosity, for determining the supernova phase, and for giving information on the rise time to maximum light.

In addition to the conventional observations, polarimetric, especially spectropolarimetric, observations of Type Ia supernovae are potentially of importance. Because of the dominance of electron opacity in the optical redward of $\sim$4000 Å, premaximum Type Ia supernova atmospheres should be highly polarizing in this wavelength region. The scenarios leading to the white dwarf explosion invoke matter accretion usually from an accretion disk. Such asymmetric accretion implies that some asymmetry, probably mostly in the outer layers, should exist in Type Ia supernovae; this asymmetry will cause the supernova flux to have a net polarization. An asymmetric burning front or mixing may also lead to asymmetries; however, given the high degree of homogeneity of Type Ia supernovae, one would not expect large asymmetries in the inner layers that control the maximum and postmaximum light behavior. A prolate or oblate asymmetry of order 10% in atmospheres with density distributions as steep as those expected for Type Ia supernovae would give rise to continuum polarization and line polarization features of only a few tenths of a percent (Shapiro & Sutherland 1982; Jeffery 1989, 1991a, b). Spectropolarimetry is of particular interest because polarization changes observed across line profiles would demonstrate intrinsic polarization and thus asymmetry despite the existence of a perhaps indeterminable amount of interstellar polarization which is slowly varying with wavelength (McCall 1984, 1985; Jeffrey 1991b). Time variation in broad-band polarimetry would also reveal asymmetry. The few broad-band polarimetric observations of Type Ia supernovae, reviewed by Shapiro & Sutherland (1982) and Barrett (1988), are inconclusive, although hints of intrinsic polarization exist. To date, there is only one Type Ia supernova with spectropolarimetry, SN 1983G (McCall et al. 1984; McCall 1985). The spectropolarimetry, taken near maximum light, showed an average polarization of 2%; the large size of this average polarization suggests that a large interstellar polarization was present. Assuming that Type Ia supernovae are standard candles, SN 1983G appears to have suffered $\sim$1 mag of extinction in the B band (Miller & Branch 1990); this implies $E(B-V) \approx 0.25$ mag. An interstellar polarization $p_{\rm ISP} = 2\%$ is then consistent with the empirical Galactic result $p_{\rm ISP} \leq 9.0E(B-V)$ of Serkowski, Mathewson, & Ford (1975). There were, however, hints of polarization features associated with P Cygni absorptions in the SN 1983G spectropolarimetry, but the uncertainty in the data points is large; consequently, one cannot conclude that intrinsic polarization was detected. Future spectropolarimetric observations should concentrate on the polarization across clean strong P Cygni lines

in the optical redward of ~4000 Å. The premaximum light epoch when the spectra form in the outer layers probably offers the best opportunity for detecting intrinsic polarization.

Some final remarks can summarize the conclusions. It seems that the model W7 Ni-Co-Fe core and intermediate-mass composition in the middle ejecta range ~9000–15,000 km s^{-1} are adquate to explain SN 1990N. For SN 1991T, a Ni-Co-Fe core and core boundary velocity of ~9000 km s^{-1} are also adequate, but the middle ejecta probably have higher iron abundance and lower intermediate-mass element abundance relative to SN 1990N and other Type Ia supernovae; nevertheless, SN 1991T is probably not fundamentally different from SN 1990N and other Type Ia's. For both SN 1990N and SN 1991T, it seems necessary to have newly synthesized elements with Ni-Co dominating the iron peak elements in the region above ~15,000 km s^{-1}. Since SN 1990N is apparently a typical Type Ia supernova and SN 1991T is probably not so far from typical, the continuation of the burning front or mixing into the outer ejecta in at least some other Type Ia supernovae must be supposed. The main challenge to those doing self-consistent and/or NLTE calculations is to test the conclusion of the necessity of newly synthesized elements in the outer ejecta and to determine accurate abundances of these elements. If the conclusion is verified, nucleosynthetic explosion models must be constructed to fit the spectrum analysis results. Given the partial success of model W7 and the delayed/late-detonation models, it is probable that some variation of these will turn out to be the correct basic Type Ia supernova model. In finding the correct basic model, more observations of Type Ia supernovae in the photospheric epoch, especially before maximum light, would be of great value.

We would like to thank Robert Kurucz for providing his line data files, Mark Phillips and Craig Foltz for providing some of their spectra of SN 1991T, and Philip Pinto for discussions. One of us (S. B.) would also like to thank the Physics and Astronomy Department of the University of Oklahoma for hospitality during his stay there. The research for this paper has been supported by NSF grant AST-89-05529 and NASA grants NAG5-841 and NAGW-1789.

REFERENCES

Ambwani, K., & Sutherland, P. G. 1988, ApJ, 325, 820
Anders, E., & Grevesse, N. 1989, Geochim. Cosmochim. Acta, 53, 197
Arnett, W. D. 1982, ApJ, 253, 785
Arnett, W. D., Branch, D., & Wheeler, J. C. 1985, Nature, 314, 337
Axelrod, T. S. 1980a, in Type I Supernovae, ed. J. C. Wheeler (Austin: Univ. Texas), 80
———. 1980b, Ph.D. thesis, Univ. California, Santa Cruz
———. 1988, in Atmospheric Diagnostics of Stellar Evolution: Chemical Peculiarity, Mass Loss, and Explosions, ed. K. Nomoto (Berlin: Springer-Verlag), 375
Barbon, R., Benetti, S., Cappellaro, E., Rosino, L., & Turatto, M. 1990, A&A, 237, 79
Barbon, R., Iijima, T., & Rosino, L. 1989, A&A, 220, 83
Barrett, P. 1988, MNRAS, 234, 937
Benetti, S., & Barbon, R. 1991, in Supernovae: The Tenth Santa Cruz Workshop in Astronomy and Astrophysics, ed. S. E. Woosley (New York: Springer-Verlag), 493
Bessell, M. S. 1990, PASP, 102, 1181
Blair, W. P., & Panagia, N. 1987, in Exploring the Universe with the *IUE* Satellite, ed. Y. Kondo, W. Wamsteker, A. Boggess, M. Grewing, C. De Jager, A. L. Lane, J. L. Linsky, & R. Wilson (Dordrecht: Reidel), 549
Branch, D. 1977, MNRAS, 179, 401
———. 1979, MNRAS, 186, 609
———. 1987, ApJ, 316, L81
———. 1992, ApJ, 392, 35
Branch, D., Doggett, J. B., Nomoto, K., & Thielemann, F.-K. 1985, ApJ, 294, 619
Branch, D., Drucker, W., & Jeffrey, D. J. 1988, ApJ, 330, L117
Branch, D., Lacy, C. H., McCall, M. L., Sutherland, P. G., Uomoto, A., Wheeler, J. C., & Wills, B. J. 1983, ApJ, 270, 123
Branch, D., & Patchett, B. 1973, MNRAS, 161, 71
Branch, D., Pauldrach, A. W. A., Puls, J., Jeffery, D. J., & Kudritzki, R. P. 1991, in ESO/EIPC Workshop: SN 1987A and Other Supernovae, ed. I. J. Danziger & K. Kjär (Garching: ESO), 437
Branch, D., & Tammann, G. A. 1992, ARA&A, 30, in press
Branch, D., & Venkatakrishna, K. L. 1986, 306, L21
Burstein, D., & Heiles, C. 1984, ApJS, 54, 33
Capaccioli, M., Cappellaro, E., Della Valle, M., D'Onofrio, Rosino, L., & Turatto, M. 1990, ApJ, 350, 110
Cardelli, J. A., Clayton, G. C., & Mathis, J. S. 1989, ApJ, 345, 245
Chilukuri, M., & Wagoner, R. V. 1988, in Atmospheric Diagnostics of Stellar Evolution: Chemical Peculiarity, Mass Loss, and Explosions, ed. K. Nomoto (Berlin: Springer-Verlag), 295
Clayton, D. D. 1983, Principles of Stellar Evolution and Nucleosynthesis (Chicago: Univ. Chicago Press)
Della Valle, M. 1991, in ESO/EIPC Workshop: SN 1987A and Other Supernovae, ed. I. J. Danziger & K. Kjär (Garching: ESO), 371
Della Valle, M., & Panagia, N. 1992, preprint
Dreiling, L. A., & Bell, R. A. 1980, ApJ, 241, 736
Eastman, R. G., & Kirshner, R. P. 1989, ApJ, 347, 771
Feldt, A. N. 1979, Proc. Oklahoma Acad. Sci., 59, 94
———. 1980, Ph.D. thesis, Univ. Oklahoma
Filippenko, A. V., et al. 1992, ApJ, 384, L15
Foltz, C. B. 1992, private communication
Hamann, W.-R. 1981, A&A, 93, 353
Hanuschik, R. W. 1991, in Supernovae: The Tenth Santa Cruz Workshop in Astronomy and Astrophysics, ed. S. E. Woosley (New York: Springer-Verlag), 26
Hanuschik, R. W., & Thimm, G. J. 1990, A&A, 231, 77
Harkness, R. P. 1986, in Radiation Hydrodynamics in Stars and Compact Objects, ed. D. Mihalas & K. H. Winkler (Berlin: Springer-Verlag), 166
———. 1991a, in Supernovae: The Tenth Santa Cruz Workshop in Astronomy and Astrophysics, ed. S. E. Woosley (New York: Springer-Verlag), 454
———. 1991b, in ESO/EIPC Workshop: SN 1987A and Other Supernovae, ed. I. J. Danziger & K. Kjär (Garching: ESO), 447
Hauschildt, P. H., Best, M., & Wehrse, R. 1991, A&A, 247, L21
Höflich, P. 1988, Proc. Astron. Soc. Australia, 7 (No. 4), 434
Huchtmeier, W. K., & Richter, O.-G. 1989, A General Catalog of HI Observations of Galaxies (New York: Springer-Verlag)
Huo, J., Hu, D., Zhou, C., Han, X., Hu, B., & Wu, Y. 1987, Nuclear Data Sheets, 51, 1
Hutsemékers, D., & Surdej, J. 1990, ApJ, 361, 367
Iye, M., Kodaira, K., Kikuchi, S., & Ohtani, H. 1975, PASJ, 27, 571
Jeffery, D. J. 1988, Ph.D. thesis, McMaster Univ.
———. 1989, ApJS, 71, 951
———. 1990, ApJ, 352, 267
———. 1991a, in ESO/EIPC Workshop: SN 1987A and Other Supernovae, ed. I. J. Danziger & K. Kjär (Garching: ESO), 257
———. 1991b, ApJ, 375, 264
Jeffery, D. J., & Branch, D. 1990, in Jerusalem Winter School for Theoretical Physics, Vol. 6, Supernovae, ed. J. C. Wheeler, T. Piran, & S. Weinberg (Singapore: World Scientific), 149
Jeffrey, D. J., & Sutherland, P. G. 1985, A&SS, 109, 277
Jöeveer, M. 1982, Astrofizika, 18, 574
Karp, A. H., Lasher, G., Chan, K. L., & Salpeter, E. E. 1977, ApJ, 214, 161
Khokhlov, A. M. 1991a, A&A, 114
———. 1991b, A&A, 245, L25
Khokhlov, A. M., Müller, E., & Höflich, P. 1992, A&A, 253, L9
Kikuchi, S. 1971, PASJ, 23, 593
Kirshner, R. P., Arp, H. C., & Dunlap, J. R. 1976, ApJ, 207, 44
Kirshner, R. P., et al. 1992, in preparation
Kirshner, R. P., & Oke, J. B. 1975, ApJ, 200, 574
Kirshner, R. P., Sonneborn, G., Crenshaw, D. M., & Nassiopoulos, G. E. 1987, ApJ, 320, 602
Kurucz, R. L. 1991, in Stellar Atmospheres: Beyond Classical Models, ed. L. Crivellari, I. Hubeny, & D. G. Hummer (Dordrecht: Kluwer), 441
Leibundgut, B. 1988, Ph.D. thesis, Univ. Basel
Leibundgut, B., Kirshner, R. P., Filippenko, A. V., Shields, J. C., Foltz, C. B., Phillips, M. M., & Sonneborn, G. 1991a, ApJ, 371, L23
Leibundgut, B., & Pinto, P. A. 1992, ApJ, in press
Leibundgut, B., & Tammann, G. A. 1990, A&A, 230, 81
———. 1992, in preparation
Leibundgut, B., Tammann, G. A., Cadonau, R., & Cerrito, D. 1991b, A&AS, 89, 537
Lucy, L. B. 1988, in Supernovae 1987A in the Large Magellanic Cloud, ed. M. Kafatos & A. G. Michalitsianos (Cambridge: Cambridge Univ. Press), 323
McCall, M. L. 1984, MNRAS, 210, 829
———. 1985, in Supernovae as Distance Indicators, ed. N. Bartel (Berlin: Springer-Verlag), 48

McCall, M. L., Reid, N., Bessell, M. S., & Wickramasinghe, D. T. 1984, MNRAS, 210, 839
Meyer, D. M., & Roth, K. C. 1991, ApJ, 383, L41
Mihalas, D. 1978, Stellar Atmospheres (San Francisco: Freeman)
Miller, D. L., & Branch, D. 1990, AJ, 100, 530
———. 1992, AJ, 103, 379
Natta, A., & Beckwith, S. 1986, A&A, 158, 310
Nomoto, K., & Hashimoto, M. 1987, Ap&SS, 131, 395
Nomoto, K., Thielemann, F.-K., & Yokoi, K. 1984, ApJ, 286, 644
Olson, G. L. 1982, ApJ, 255, 267
Panagia, N., & Gilmozzi, R. 1991a, in Supernovae: The Tenth Santa Cruz Workshop in Astronomy and Astrophysics, ed. S. E. Woosley (New York: Springer-Verlag), 497
———. 1991b, in ESO/EIPC Workshop: SN 1987A and Other Supernovae, ed. I. J. Danziger & K. Kjär (Garching: ESO), 575
Peletier, R. F., & Willner, S. P. 1991, ApJ, 382, 382
Phillips, M. M., & Heathcote, S. R. 1989, 101, 137
Phillips, M. M., et al. 1987, PASP, 99, 592
Phillips, M. M., Wells, L. A., Suntzeff, N. B., Hamuy, M., Leibundgut, B., Kirshner, R. P., & Foltz, C. B. 1992, AJ, 103, 1632
Pierce, M. J., & Tully, R. B. 1988, ApJ, 330, 579
Ruiz-Lapuente, P., Cappellaro, E., Turatto, M., Gouiffes, C., Danziger, I. J., Della Valle, M., & Lucy, L. B. 1992, ApJ, 387, L33
Rybicki, G. B., & Hummer, D. G. 1978, ApJ, 219, 654
Schmidt, B. P., Kirshner, R. P., & Eastman, R. G. 1992, ApJ, 395, 366
Schmutz, W., Abbot, D. C., Russell, R. S., Hamann, W.-R., & Wessolowsky, U. 1990, ApJ, 355, 255
Serkowski, K., Mathewson, D. S., & Ford, V. L. 1975, ApJ, 196, 261
Shapiro, P. R., & Sutherland, P. G. 1982, AJ, 263, 902
Shigeyama, T., Nomoto, K., Yamaoka, H., & Thielemann, F.-K. 1992, ApJ, 386, L13
Smith, V., & Wheeler, J. C. 1991, IAU Circ., No. 5256
Sutherland, P. G., & Wheeler, J. C. 1984, ApJ, 280, 282
Thielemann, F.-K. 1992, private communication
Thielemann, F.-K., Nomoto, K., & Yokoi, K. 1986, A&A, 158, 17
Tully, R. B., Shaya, E. J., & Pierce, M. J. 1992, ApJS, 80, 479
Wegner, G., & McMahan, R. K. 1987, AJ, 93, 287
Wheeler, J. C., & Harkness, R. P. 1990, Rep. Prog. Phys., 53, 1467
Wheeler, J. C., Harkness, R. P., Barkat, Z., & Swartz, D. 1986, PASP, 98, 1018
Woosley, S. E. 1990, in Supernovae, ed. A. G. Petschek (New York: Springer-Verlag), 182
———. 1991, in Gamma-Ray Line Astrophysics, ed. P. Durouchoux & N. Prantzos (Paris: AIP), 270
Woosley, S. E., & Weaver, T. A. 1986a, ARA&A, 24, 205
———. 1986b, in IAU Symp. 89, Radiation Hydrodynamics in Stars and Compact Objects, ed. D. Mihalas & K.-H. Winkler (Berlin: Springer-Verlag), 91
Yamaoka, H., Nomoto, K., Shigeyama, T., & Thielemann, F.-K. 1992, ApJ, 393, L55